lurethane (*bis*-THF), which forms a number of strong hydrogen bonds, via ligand oxygen atoms, with the backbone atoms of the active site of HIV-1 protease. Furthermore, the bicyclic ligand effectively fills the hydrophobic pocket in the S2 subsite.[10,11]

Based on X-ray structural insight into the molecular interactions of *bis*-THF, we subsequently planned to investigate the effect of fluorine atoms at the C4 position of the *bis*-THF ring.[12] In particular, we speculated that fluorine would increase lipophilicity, which in turn may improve drug penetration in the central nervous system (CNS). Because the CNS is a major sanctuary for HIV-1 infection, improving drug concentration in the CNS may be an important strategy to decrease HIV-1-associated dementia and other CNS-related disorders.[13,14] With prolonged patient survival, HIV-1-associated neurocognitive disorders (HAND) are increasing, possibly due to poor CNS penetration of current anti-HIV therapies.[15] Furthermore, sub-therapeutic drug concentrations in the CNS may also play a role in the development of viral resistance.[16] Although combined antiretroviral therapy (cART) has been effective in decreasing morbidity and mortality in HIV/AIDS patients, currently there appears to be no readily feasible therapy for the cure or eradication of HIV, in part due to viral reservoirs in tissues and the CNS.

In our structure-based design strategies, we plan to preserve key backbone hydrogen bonding interactions through *bis*-THF ring oxygen atoms. We also presume that our structure-based fluorine substitution may improve molecular binding properties in the HIV-1 protease active site through noncovalent interactions involving fluorine.[17,18] This may result in potent antiviral activity against multi-drug-resistant HIV-1 variants. Herein we report an enantioselective synthesis of *gem*-difluoro-*bis*-THF ligands and their conversion into *gem*-difluoro-*bis*-THF containing HIV-1 PIs resembling darunavir. We also carried out X-ray structural studies of inhibitor-bound HIV-1 protease and the biological evaluation of inhibitors.

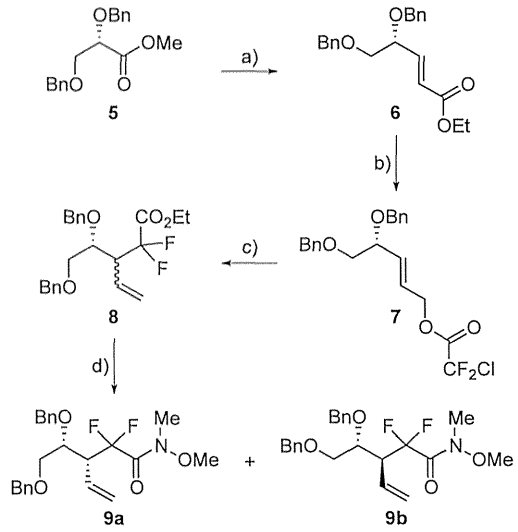


**Scheme 1.** Reformatskii–Claisen route to *gem*-difluoro derivatives **9a,b**. *Reagents and conditions*: a) 1. DIBAL-H, −78 °C, 1.5 h, 2. $(EtO)_2P(O)CH_2CO_2Et$, NaH, THF, 0 °C, 30 min, 88% (two steps); b) 1. DIBAL-H, −78 °C, 4 h, 2. $ClCF_2CO_2H$, reflux, 10 h, 90% (two steps); c) 1. Zn, TMSCl, 105 °C, 24 h, 2. $H_2SO_4$ (cat.), EtOH, 50 °C, 36 h, 80% (two steps); d) HNMe(OMe)·HCl, *n*BuLi, THF, −78 °C, 3 h, 90%.

## Synthesis of Ligands and Inhibitors

The synthesis of stereochemically defined *gem*-difluoro derivatives of *bis*-THF is shown in Scheme 1. As shown, diisobutylaluminum hydride (DIBAL-H) reduction of optically active methyl ester **5** provided dibenzyl-L-glyceraldehyde.[19] Horner–Emmons reaction of the resulting aldehyde with sodium hydride and triethyl phosphonoacetate afforded α,β-unsaturated ester **6** in 88% yield over two steps. Notably, the crude dibenzyl-L-glyceraldehyde was employed immediately to Horner–Emmons reaction without purification to avoid racemization of the aldehyde. Reduction of α,β-unsaturated ester **6** with DIBAL-H in dichloromethane at −78 °C provided the corresponding allylic alcohol.[20] Treatment of the resulting alcohol with chlorodifluoroacetic acid in chloroform at reflux afforded difluoroacetate derivative **7** in 90% yield over two steps. The optical rotation of ester **6** ($[\alpha]_D^{23} = -15.4$ ($c = 1.08$, $CHCl_3$)) was similar to the reported value for the corresponding enantiomeric ester (lit.[20] $[\alpha]_D^{23} = +13.4$ ($c = 1.75$, $CHCl_3$)). Ester **7** was then subjected to Reformatskii–Claisen reaction[21,22] by treatment with trimethylsilyl chloride (TMSCl) and activated zinc dust in acetonitrile at reflux for 24 h. Subsequent esterification of the crude acid product with a catalytic amount of concentrated sulfuric acid in ethanol at 50 °C furnished a 2:1 mixture (by $^1H$ NMR analysis) of diastereomers **8** in 80% yield over two steps. This mixture could not be separated by silica gel column chromatography. However, the mixture could be separated after its conversion into the Weinreb amides. Thus, reaction of the mixture **8** with HN(Me)OMe·HCl and *n*BuLi in THF at −78 °C for 3 h provided the corresponding mixture of Weinreb amides. These amide diastereomers were separated by silica gel chromatography to provide *syn* diastereomer **9a** as the major product and *anti* diastereomer **9b** as the minor product in a 2:1 ratio and 80% combined yield. The assignment of stereochemistry was based on reported $^1H$ NMR data for the corresponding enantiomer.[20]

Both *syn* diastereomer **9a** and *anti* diastereomer **9b** were converted into the respective *gem*-difluoro derivatives of *bis*-THF as shown in Scheme 2. Reduction of Weinreb amide **9a** was carried out with lithium aluminum hydride in THF at −78 °C, and the resulting crude aldehyde was reduced with the addition of sodium borohydride in a one-pot operation to provide difluoro alcohol **10** in near quantitative yield. Ozonolysis of the olefin in **10** followed by reductive cleavage with triphenylphosphine provided crude cyclic acetal **11** upon cyclization. The crude cyclic acetal was purified in a short silica gel column using dichloromethane as eluent. The resulting cyclic acetal was then subjected to catalytic hydrogenation over Pearlman's catalyst under a hydrogen-filled balloon in ethyl acetate to furnish the corresponding triol. Treatment of the resulting triol with a catalytic amount of camphorsulfonic acid (CSA) in THF and dichloromethane at 23 °C for 12 h afforded

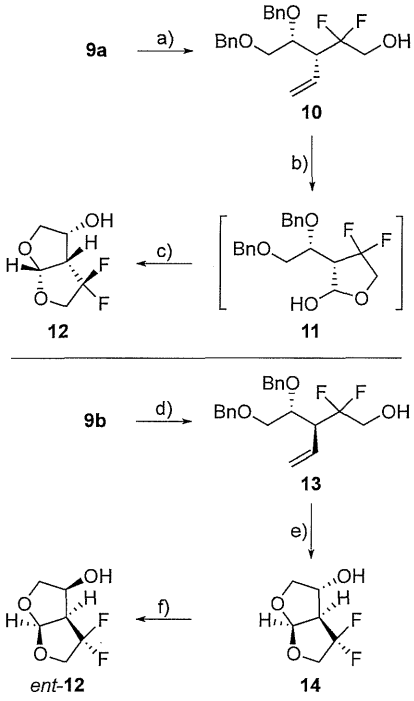


**Scheme 2.** Synthesis of *gem*-difluoro *bis*-THF derivatives **12** and *ent*-**12**. *Reagents and conditions*: a) $LiAlH_4$, THF, 0 °C, 30 min, then $NaBH_4$, overnight, 99%; b) $O_3$, $CH_2Cl_2$, −78 °C, 5 min, then $PPh_3$, −78 °C, 2 h, then 23 °C, 3 h; c) 1. $H_2$, Pd/C, overnight, 2. CSA (cat.), THF/$CH_2Cl_2$, overnight, 68% (three steps); d) $LiAlH_4$, THF, 0 °C, 30 min, then $NaBH_4$, overnight, 96%; e) 1. $O_3$, $CH_2Cl_2$, −78 °C, 5 min, then $PPh_3$, −78 °C, 2 h, then 23 °C, 3 h; 2. $H_2$, Pd/C, overnight, 3. CSA (cat.), THF/$CH_2Cl_2$, overnight, 73% (three steps); f) 1. Dess–Martin, 23 °C, 2 h, 2. L-selectride, −78 °C, 30 min, 82% (two steps).

optically active difluoro-*bis*-THF **12** in 68% yield over three steps. Anti-diastereomer **9b** was converted into its corresponding enantiomeric ligand. Weinreb amide **9b** was reduced to alcohol **13**, which was converted into the corresponding difluoro-*bis*-THF derivative **14** by following the same reaction sequence as for the synthesis of **12**. *bis*-THF derivative **14** was obtained in 73% yield over three steps from alcohol **13**. This was converted into the enantiomer of **12** (*ent*-**12**) by Dess–Martin oxidation followed by reduction with L-selectride in THF at −78 °C, providing *ent*-**12** in 82% yield over two steps.

The synthesis of inhibitors containing difluoro-*bis*-THF ligands is shown in Scheme 3. Both *bis*-THF enantiomers and alcohol **14** were treated with *para*-nitrophenyl chloroformate in dichloromethane in the presence of pyridine at 0 °C to 23 °C for 12 h to provide the corresponding activated carbonate **15**, *ent*-**15**, and **16**, respectively.[23] These activated carbonates were reacted with known (*R*)-hydroxyethylsulfonamide isostere **17**[23] in the presence of triethylamine to furnish inhibitors **3**, **19**, and **20** in good yields. Treatment of known amine **18**[24] and activated carbonates **15** and **16** provided inhibitors **4** and **21** in good yield.

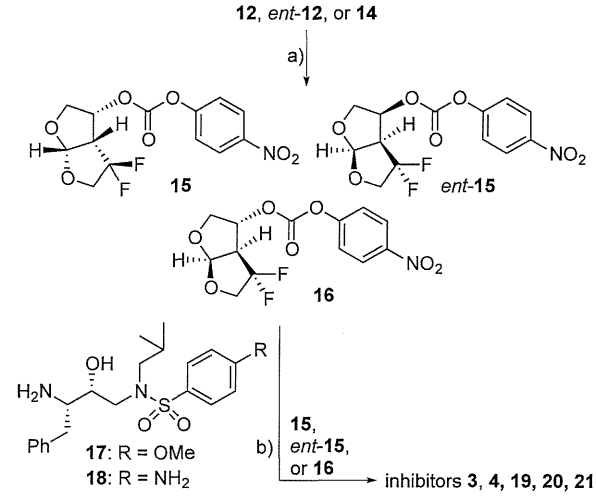


**Scheme 3.** Synthesis of inhibitors **3**, **4**, **19**, **20**, and **21** with *gem*-difluorides. *Reagents and conditions*: a) *p*-$NO_2$-PhOCOCl, pyridine, $CH_2Cl_2$, 23 °C, 2 h; b) $Et_3N$, 3 days.

## Results and Discussion

Our examination of the X-ray crystal structure of darunavir-bound HIV-1 protease[12] and subsequent modeling suggested that substitution of fluorine at the C4 position of the *bis*-THF ligand may lead to strong non-bonding interactions with the carbonyl oxygen atom of Gly48. Fluorine may effectively fill the hydrophobic pocket in the S2 site as well. For synthesis and stability purposes, we designed *gem*-difluoride at the C4 position. As it is evident in Table 1, two fluoro-*bis*-THF-derived inhibitors showed exceptional enzyme inhibitory potency, as determined by the assay protocol reported by Toth and Marshall.[25] Inhibitor **3**, with *para*-methoxyphenylsulfonamide as the P2′ ligand, showed a $K_i$ value of 22 pM. The corresponding *para*-amino derivative **4** displayed a $K_i$ value of 5.8 pM. The enantiomeric fluoro *bis*-THF group as P2 ligand and *para*-methoxysulfonamide as the P2′ ligand provided inhibitor **19**. This inhibitor showed a significant decrease in inhibitory potency. Furthermore, a C3 epimeric ligand at P2 and *para*-methoxy sulfonamide as the P2′ ligand resulted in inhibitor **20**, with a dramatic increase in enzyme $K_i$. Antiviral activity of these *gem*-difluoro derivatives was determined in MT-2 human T-lymphoid cells exposed to $HIV_{LAI}$.[26] As shown, inhibitors **3** and **4** displayed $IC_{50}$ values of 0.0008 and 0.003 μM, respectively. In comparison, darunavir and saquinavir showed respective antiviral $IC_{50}$ values of 0.005 and 0.021 μM. Inhibitor **19** showed significantly lower antiviral activity than inhibitor **3**. Inhibitor **21** was found to be inactive in our antiviral assay. Inhibitors **3** and **4** showed cytotoxicity only at high concentrations, with $CC_{50}$ values of 17.5 and 37 μM, respectively. The respective selectivity indexes ($CC_{50}/IC_{50}$) for compounds **3** and **4** were 21875 and 12333. In comparison, darunavir showed a selectively index of >20000.

We then examined inhibitors **3** and **4** against clinical wild-type X4 HIV-1 isolate ($HIV\text{-}1_{ERS104pre}$) along with a panel of highly multi-PI-resistant primary HIV-1 strains, $HIV\text{-}1_{MDR/B}$ (multi-

**Table 1.** Enzyme inhibitory and antiviral activity of difluoro-*bis*-THF-derived inhibitors.

| Inhibitor | $K_i$ [nM][a] | $IC_{50}$ [μM][b] |
|---|---|---|
| 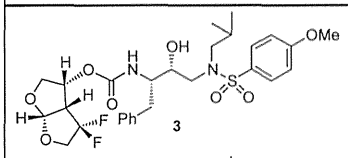 **3** | 0.022 | 0.0008 |
| 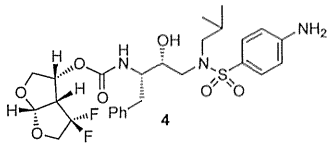 **4** | 0.0058 | 0.0031 |
| 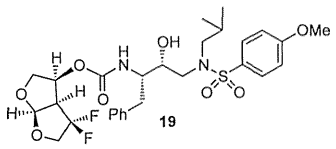 **19** | 0.21 | 0.02 |
| 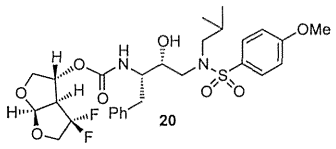 **20** | 3.9 | 0.64 |
| 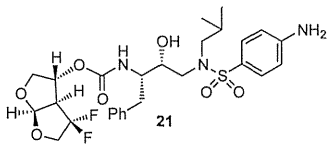 **21** | 5.14 | >1.0 |

[a] $K_i$ values are the mean of at least five data points; standard error in all cases was <7%. Darunavir: $K_i$=16 pM. [b] Values are the mean of at least three experiments. Human T-lymphoid (MT-2) cells were exposed to 100 $TCID_{50}$ values of HIV-1 LAI and cultured in the presence of each PI, and the $IC_{50}$ values were determined by MTT assay. Standard error in all cases was <5%. Darunavir: $IC_{50}$=1.6 nM.

drug resistant, MDR), HIV-$1_{MDR/C}$, HIV-$1_{MDR/G}$, HIV-$1_{MDR/TM}$, and HIV-$1_{MDR/JSL}$, as listed in Table 2. These were isolated from HIV/AIDS patients who had failed a number of anti-HIV therapeutic regimens after receiving 9–11 anti-HIV drugs over 32–83 months.[27] These primary strains possessed 9–14 residue substitutions in the protease-encoding region of the HIV-1 genome. These substitutions have been associated with HIV-1 resistance against various approved PIs, and are noted in the footnote of Table 2. As can be seen, the $EC_{50}$ values of both inhibitors **3** and **4** are significantly more potent than that of amprenavir (APV) and are similar to the potency of darunavir (DRV) against wild-type HIV-$1_{ERS104pre}$, using PHA-PBMC as target cells and p24 production as the endpoint. Interestingly, both PIs **3** and **4** displayed $EC_{50}$ values ranging from 0.021 to 0.002 μM against the panel of six MDR clinical HIV-1 variants. In comparison, APV was less active, with $EC_{50}$ values and fold differences ranging between 0.21 and 0.63 μM, and 7–22-fold, respectively. The $EC_{50}$ values of inhibitors **3** and **4** are similar to, or better than, the activity of DRV against this panel of variants.

Both inhibitors **3** and **4** are also effective against PI-selected laboratory HIV-1 variants; a detailed study was reported recently.[28] We also evaluated apparent blood–brain barrier (BBB) permeability coefficients of inhibitors **3** and **4** and compared these against that of darunavir. The assay protocol involved a triple cell co-culture system with rat astrocytes, pericytes, and monkey endothelial cells. The model kit represents an in vitro BBB model for drug transport assay, as described by Nakagawa and co-workers.[29] In this assay, test inhibitor was added to the luminal interface (termed the blood side) of the microtiter culture wells under the conditions optimal for trans-endothelial electrical resistance (TEER) determination. The concentration of each inhibitor that permeated into the abluminal interface (termed brain side) was determined spectrophotometrically 30 min after the addition of each inhibitor to the wells. As listed in Table 3, both fluorinated inhibitors **3** and **4** showed significantly higher drug concentrations in the abluminal interface of the microtiter culture wells than darunavir (0.62 μM). The apparent permeability coefficient ($P_{app}$) is referred to as a brain uptake index. It is a way to measure the penetration efficiency of a drug across the BBB model quantitatively and qualitatively.[30] As can be seen, both fluoro derivatives **3** and **4** showed $P_{app}$ values significantly better than the $P_{app}$ values of DRV.

To obtain molecular insight into the interactions of fluorinated inhibitors, we co-crystallized inhibitor **4** (GRL-05010) with HIV-1 protease, and the resulting structure was refined at the high resolution of 1.3 Å (PDB ID: 4U8W). The structure contains the HIV-1 protease dimer and the inhibitor with orientations related by 180° rotation with 55/45% relative occupancies. The protease dimer structure closely resembles our previously reported structure of the protease–darunavir complex with an RMSD of 0.19 Å for all Cα atoms.[12] Because this inhibitor is a difluorinated derivative of darunavir, the majority of inhibitor interactions in the active site are similar to those of darunavir. As shown in Figure 2, the inhibitor is bound in the active site cavity through a network of strong hydrogen bonding interactions with backbone atoms, as well as with the catalytic aspartate groups of HIV-1 protease. Both oxygen atoms of the *bis*-THF ligand form strong hydrogen bonds with the backbone amides of Asp30 and Asp29. Interestingly, both fluorine atoms on the *bis*-THF ligand form strong interactions with the carbonyl oxygen atom of Gly48, as shown. For the major conformation, these interactions show short distances of 2.2 and 2.6 Å; for the minor conformation, these were 2.6 and 2.8 Å. Similar interactions of a fluorine atom with a carbonyl oxygen of various amino acids have been observed previously in various protein structures, with a frequency of >9%.[17] Because Gly48 is located in the flap, for inhibitor **3**, these F···OC interactions with Gly48 may tend to stabilize the flexible flap region as well as improve the binding affinity for the HIV-1 protease complex. The structure also shows hydrogen bonding interactions of the carbamate NH group with the backbone carbonyl oxygen atom of Gly27. The amine functionality of the P2′ ligand forms a strong hydrogen bond with Asp30′ NH, as well as with the side chain carboxylic acid of Asp30′. Furthermore, the inhibitor forms water-mediated interactions with the carbamate carbonyl oxygen, sulfonamide oxygen, and the amides of Ile50 and Ile50′ in the flaps of HIV-1 protease. Similar interactions are inherent to the darunavir-bound HIV-1 protease X-ray

**Table 2.** Antiviral activity of PIs **3** and **4** against multi-drug-resistant clinical isolates in PHA-PBMs.[a]

| Virus (phenotype) | $EC_{50}$ [μM][b] APV | DRV | **3** (GRL-04810) | **4** (GRL-05010) |
|---|---|---|---|---|
| HIV-$1_{ERS104pre}$ (wild-type X4) | 0.0299±0.0067 | 0.0037±0.0001 | 0.0023±0.0001 | 0.0029±0.0005 |
| HIV-$1_{MDR/B}$ (X4) | 0.4892±0.0536 (16) | 0.0276±0.0043 (7) | 0.0204±0.0065 (9) | 0.0212±0.0086 (7) |
| HIV-$1_{MDR/C}$ (X4) | 0.2720±0.0199 (9) | 0.0175±0.0049 (5) | 0.0068±0.0001 (3) | 0.0051±0.0011 (2) |
| HIV-$1_{MDR/G}$ (X4) | 0.3373±0.0950 (11) | 0.0189±0.0054 (5) | 0.0041±0.0015 (2) | 0.0043±0.0009 (1) |
| HIV-$1_{MDR/TM}$ (X4) | 0.3656±0.0362 (12) | 0.0279±0.0140 (8) | 0.0045±0.0017 (2) | 0.0051±0.0021 (2) |
| HIV-$1_{MDR/JSL}$ (R5) | 0.5713±0.0844 (19) | 0.0261±0.0054 (7) | 0.0218±0.0076 (9) | 0.0213±0.0018 (7) |

[a] The amino acid substitutions identified in the protease-encoding region of HIV-$1_{ERS104pre}$, HIV-$1_B$, HIV-$1_C$, HIV-$1_G$, HIV-$1_{TM}$, HIV-$1_{JSL}$ compared with the consensus type B sequence cited from the Los Alamos database include L63P; L10I, K14R, L33I, M36I, M46I, F53I, K55R, I62V, L63P, A71V, G73S, V82A, L90M, I93L; L10I, I15V, K20R, L24I, M36I, M46L, I54V, I62V, L63P, K70Q, V82A, L89M; L10I, V11I, T12E, I15V, L19I, R41K, M46L, L63P, A71T, V82A, L90M; L10I, K14R, R41K, M46L, I54V, L63P, A71V, V82A, L90M, I93L; and L10I, L24I, I33F, E35D, M36I, N37S, M46L, I54V, R57K, I62V, L63P, A71V, G73S, V82A, respectively. HIV-$1_{ERS104pre}$ served as a source of wild-type HIV-1. [b] $EC_{50}$ values were determined by using PHA-PBMs as target cells, and the inhibition of p24 Gag protein production by each drug was used as an endpoint. Numbers in parentheses represent the fold change in $EC_{50}$ value for each isolate relative to the $IC_{50}$ values for wild-type HIV-$1_{ERS104pre}$. All assays were conducted in duplicate, and the data shown represent mean values (±1 SD) derived from the results of two or three independent experiments.

**Table 3.** Apparent permeability blood–brain barrier coefficient for inhibitors **3** and **4** in an in vitro model.[a]

| Compd | Concentration [μM] Initial luminal tracer | Final abluminal tracer | $P_{app}$ [$10^{-6}$ cm $s^{-1}$] |
|---|---|---|---|
| GRL-04810 | 100 | 3.33±0.70 | 50.38±10.61 |
| GRL-05010 | 100 | 4.01±0.27 | 60.84±3.97 |
| DRV | 100 | 0.62±0.15 | 9.32±2.25 |

[a] In the in vitro model using a triple co-culture of rat astrocytes, pericytes, and monkey endothelial cells, GRL-04810, GRL-05010, DRV (all 100 μM) were added to the luminal interface (termed blood side) of duplicate wells. The mathematical formula used for the calculation of $P_{app}$ is described in the Experimental Section. Results shown are the average values ±1 SD of duplicate determinations.

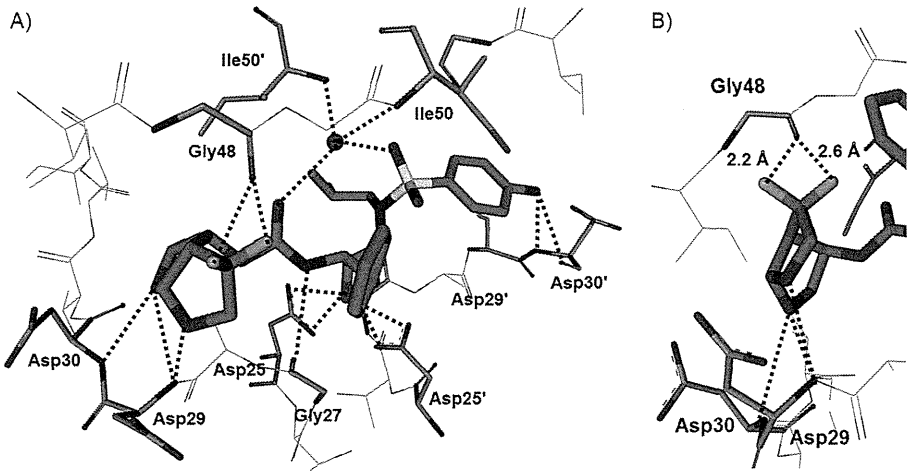


**Figure 2.** A) GRL-05010A-bound X-ray structure of HIV-1 protease. The major orientation of the inhibitor is shown. The inhibitor carbon atoms are shown in green, water molecules are red spheres, and the hydrogen bonds are indicated by dotted lines. B) Non-bonded interactions of *gem*-difluorides with the carbonyl group of Gly48 in the protease flap region; these interactions are indicated with their respective distances.

structure. Both P1 and P2′ aromatic rings, as well as the P1′ isobutyl side chain effectively fill the hydrophobic pockets of HIV-1 protease in S1, S2′, and S1′ subsites, respectively. These extensive molecular interactions, including F···OC interactions, may be responsible for the high affinity of these inhibitors for HIV-1 protease and their robust potency against drug-resistant HIV-1 variants.

## Conclusions

We have investigated fluorine-containing inhibitors to improve brain penetration. In this context, we incorporated *gem*-difluorides based on the X-ray structure of darunavir-bound HIV-1 protease. The corresponding *gem*-difluoro-*bis*-THF ligand was synthesized stereoselectively through a Reformatskii–Claisen reaction as the key step. Both enantiomers of *bis*-THF ligand were synthesized in the optically active form. These fluoro derivatives were then incorporated in the (*R*)-hydroxyethylsulfonamide isostere. The absolute stereochemistry of the P2-fluoro-*bis*-THF ligand was critical to the potency of the inhibitors. Consistent with our previous studies, the ligand containing (3*R*,3a*S*,6a*R*)-*bis*-THF displayed enhanced enzyme inhibitory and antiviral potency relative to the enantiomeric ligand. Both inhibitors **3** and **4** maintained excellent antiviral activity against a variety of multidrug-resistant clinical HIV-1 variants, with $EC_{50}$ values ranging from 0.021 to 0.002 μM. These values are significantly better than those observed for amprenavir and are similar to or better than that of darunavir. Of particular note, both inhibitors showed much improved BBB permeability coefficients relative to darunavir in an in vitro model. A high-resolution X-ray crystal structure of inhibitor **4**-bound HIV-1 protease revealed that the fluoro-*bis*-THF ligand is involved in extensive interactions in the S2 subsite, including a number of critical hydrogen bonding interactions with Asp29 and Asp30 backbone NHs. Also, both *gem*-difluorides form strong interactions with the Gly48 carbonyl oxygen located in the flap region of HIV-1 protease. These interactions are likely responsible for the exceptional activity of

these inhibitors, which are particularly active against a wide spectrum of drug-resistant HIV-1 variants. Our current results warrant further investigation.

## Experimental Section

All moisture-sensitive reactions were carried out in an oven-dried flask under an argon atmosphere. Anhydrous solvents were obtained as follows: THF, $Et_2O$, and benzene were distilled from sodium and benzophenone; $CH_2Cl_2$, pyridine, $CH_3CN$, $Et_3N$, and *N,N*-diisopropylethylamine, distilled from $CaH_2$. All other solvents were HPLC grade. $^1H$ NMR and $^{13}C$ NMR spectra were recorded on Varian INOVA300-1 and Bruker Avance ARX-400 spectrometers. NMR data were resolved with MestReNova 9.0.1 software. Optical rotations were recorded on a PerkinElmer 341 polarimeter. Mass spectra were obtained at the Purdue University Campus-wide Mass Spectrometry Center. Column chromatography was performed with Whatman 240–400 mesh silica gel under a low pressure of 3–5 psi. TLC was carried out with E. Merck silica gel 60 $F_{254}$ plates. HPLC was performed on an Agilent 1100 instrument. All test inhibitors showed purity >96% by HPLC analysis.

**Ethyl (*R,E*)-4,5-*bis*(benzyloxy)pent-2-enoate (6):** Methyl ester **5** (3.01 g, 10 mmol) was dissolved in $CH_2Cl_2$ (50 mL) and cooled to −78 °C. To the solution was added DIBAL (1.0 M in $CHCl_2$, 15 mL, 15 mmol), and the mixture was stirred for 1.5 h. The reaction was quenched with saturated aqueous Rochelle salt, and the mixture was stirred overnight until the aqueous phase became clear. The organic phase was then washed with brine, dried over sodium sulfate, filtered, and evaporated in vacuo to give the corresponding crude aldehyde (2.85 g). The aldehyde was immediately subjected to the next Horner–Emmons reaction.

A suspension of NaH (60% dispersion in mineral oil, 1.48 g, 37.0 mmol) in THF (30 mL) was cooled to 0 °C. Triethyl phosphonoacetate (7.95 mL, 40.1 mmol) was added dropwise to the above suspension. After 30 min, the above aldehyde was added, and the mixture was stirred for 1 h. The reaction mixture was neutralized with saturated aqueous $NH_4Cl$ and extracted with EtOAc. The organic layer was washed with brine, dried over $Na_2SO_4$, filtered, and evaporated in vacuo. The residue was purified by silica gel chromatography (hexanes/EtOAc 20:1) to give unsaturated ethyl ester **6** (2.99 g, 8.78 mmol, 88% for two steps) as a colorless oil. $^1H$ NMR spectra are consistent with those reported ($[\alpha]_D^{23} = -23.4$ ($c = 1.39$, $CHCl_3$; lit.[20] $[\alpha]_D^{23} = +19.2$ ($c = 1.45$, $CHCl_3$)).

**(*R,E*)-4,5-*bis*(Benzyloxy)pent-2-en-1-yl 2-chloro-2,2-difluoroacetate (7):** α,β-Unsaturated ester **6** (2.96 g, 8.7 mmol) was dissolved in dry, distilled $CH_2Cl_2$ (50 mL), and the solution was cooled to −78 °C. To this cold reaction mixture, DIBAL-H (1.0 M in $CH_2Cl_2$, 34.8 mL) was added dropwise. The resulting mixture was stirred for 4 h. After this period, the reaction was quenched with saturated aqueous Rochelle salt at −78 °C, and the mixture was warmed to 23 °C; stirring continued for 12 h until the aqueous phase became clear. The organic phase was extracted with EtOAc. The organic layer was washed with brine, dried over $Na_2SO_4$, filtered, and evaporated in vacuo to yield the crude allylic alcohol, which was used directly without further purification.

The crude allylic alcohol was dissolved in $CHCl_3$ (50 mL), and chlorodifluoroacetic acid (3.67 mL, 43.45 mmol) was added. The resulting mixture was stirred at reflux for 10 h. After this period, the reaction mixture was cooled to 23 °C and extracted with $CH_2Cl_2$. The organic phase was washed with brine, dried with anhydrous $Na_2SO_4$, filtered and evaporated in vacuo. The crude residue was purified by silica gel chromatography (hexanes/EtOAc 15:1) to provide the title compound **7** (3.2 g, 90% over two steps); $[\alpha]_D^{23} = -15.4$ ($c = 1.08$, $CHCl_3$); $^1H$ NMR (400 MHz, $CDCl_3$): $\delta = 7.35–7.30$ (m, 10H), 5.89–5.87 (m, 2H), 4.83 (d, $J = 3.92$ Hz, 1H), 4.63 (d, $J = 11.84$ Hz, 1H), 4.51 (s, 2H), 4.50 (d, $J = 11.84$ Hz, 1H), 4.10–4.08 (m, 1H), 3.59 (dd, $J = 10.2$ Hz, 6.1 Hz, 1H), 3.52 ppm (dd, $J = 10.2$ Hz, 4.7 Hz, 1H); $^{13}C$ NMR (75.5 MHz, $CDCl_3$): $\delta = 158.9$, 137.9, 137.8, 134.6, 132.7, 129.8, 129.0, 128.4, 127.7, 127.7, 124.9, 116.8, 78.2, 76.7, 73.4, 72.8, 72.4, 71.0, 70.6, 67.6 ppm.

**Ethyl (*R*)-4,5-bis(benzyloxy)-2,2-difluoropentanoate (8):** The above chlorodifluoroacetate derivative **7** (1.68 g, 4.45 mmol) and chlorotrimethylsilane (0.76 mL, 6 mmol) were dissolved in dry distilled $CH_3CN$ (40 mL). To this mixture activated Zn dust (2.9 g, 44.6 mmol) was added, and the resulting mixture was heated at 105 °C for 24 h. After this period, the reaction mixture was cooled to 23 °C and filtered through a pad of Celite. The solvent was removed in vacuo, and the residue was dissolved in EtOH (40 mL), concentrated $H_2SO_4$ (1.1 mL) was added, and the mixture was stirred for 36 h at 50 °C. After this period, the reaction mixture was concentrated, and the residue was diluted with water. It was then extracted with hexane, dried over $Na_2SO_4$, filtered, and evaporated to dryness. The residue was purified by silica gel chromatography (hexanes/EtOAc 30:1) to afford compound **8** (1.44 g, 80%) as a diastereomeric mixture (2:1 by $^1H$ NMR). $^1H$ NMR (400 MHz, $CDCl_3$): $\delta = 7.34–7.25$ (m, 15H), 5.92 (dt, $J = 17.2$ Hz, 9.9 Hz, 1H) major, 5.66 (m, 1H) minor, 5.32 (dd, $J = 8.8$ Hz, 0.9 Hz, 2H) major, 5.23–5.19 (m, 2H) minor, 4.68–4.63 (m, 2H) minor, 4.56–4.42 (m, 2H) major, 4.10–4.04 (m, 3H), 3.89–3.86 (m, 1H) major, 3.59–3.56 (m, 1H) minor, 3.52–3.51 (m, 1H) minor, 3.44 (dd, $J = 9.5$ Hz, 6.9 Hz, 1H) major, 1.20 (t, $J = 7.28$, 3H) major, 1.09 ppm (t, $J = 7.08$, 3H) minor; $^{13}C$ NMR (75.5 MHz, $CDCl_3$): $\delta = 138.1$, 137.9 minor, 128.6, 128.3, 128.1, 128.1, 127.6, 122.8, 122.6, 74.9, 73.2, 72.8, 72.5, 69.8, 62.6, 62.2, 51.3, 13.7, 13.6 ppm.

**(*R*)-3-((*R*)-1,2-*bis*(Benzyloxy)ethyl)-2,2-difluoro-*N*-methoxy-*N*-methylpent-4-enamide (9a) and (*S*)-3-((*R*)-1,2-*bis*(benzyloxy)ethyl)-2,2-difluoro-*N*-methoxy-*N*-methylpent-4-enamide (9b):** To a suspension of *N,O*-dimethylhydroxylamine hydrochloride (1.7 g, 17.5 mmol) in THF (40 mL) at −78 °C, *n*BuLi (22 mL, 1.6 M in hexane) was added. The resulting reaction mixture was stirred for 1 h at this temperature. To this reaction mixture, a solution of compound **8** (1.42 g, 3.51 mmol) in THF (10 mL) was added via cannula. The reaction was monitored by TLC, and after 2 h the reaction was quenched at −78 °C using saturated aqueous $NH_4Cl$ solution. The resulting mixture was warmed to 23 °C. The reaction mixture was extracted with EtOAc, washed with brine, dried over $Na_2SO_4$ and concentrated in vacuo. The crude residue was purified by silica gel chromatography (hexanes/EtOAc 10:1) to afford **9a** (0.80 g, 1.88 mmol) and **9b** (0.40 g, 0.94 mmol) in a 2:1 ratio in 81% overall yield.

**9a**: $[\alpha]_D^{23} = -25.1$ ($c = 1.07$, $CHCl_3$); $^1H$ NMR (400 MHz, $CDCl_3$): $\delta = 7.35–7.25$ (m, 10H), 5.92 (dt, $J = 17.2$ Hz, 9.9 Hz, 1H), 5.31 (dd, $J = 10.3$ Hz, 0.9 Hz, 1H), 5.19 (d, $J = 17.3$ Hz, 1H), 4.65 (dd, $J = 15.2$ Hz, 11.3 Hz, 2H), 4.54 (d, $J = 11.8$ Hz, 1H), 4.45 (d, $J = 11.9$ Hz, 1H), 4.03 (bs, 1H), 3.68 (s, 3H), 3.60 (dt, $J = 11.5$ Hz, 4.45 Hz, 1H), 3.50 (dd, $J = 9.7$ Hz, 6.4 Hz, 1H), 3.42–3.37 (m, 1H), 3.13 ppm (s, 3H).

**9b**: $[\alpha]_D^{23} = -18.0$ ($c = 0.55$, $CHCl_3$); $^1H$ NMR (400 MHz, $CDCl_3$): $\delta = 7.36–7.24$(m, 10H), 5.71 (dt, $J = 16.7$ Hz, 10.5 Hz, 1H), 5.33 (s, 1H), 5.30 (d, $J = 11.2$ Hz, 1H), 4.66 (d, $J = 10.8$ Hz, 1H), 4.50 (dd, $J = 12.1$ Hz, 5.5 Hz, 2H), 4.42 (d, $J = 10.7$ Hz, 1H), 3.79–3.75 (m, 1H), 3.69–3.65 (m, 1H), 3.62 (s, 3H), 3.59–3.51(m, 1H), 3.46 (dd, $J = 10.6$ Hz, 4.7 Hz, 1H), 2.78 ppm (bs, 3H).

**(*R*)-3-((*R*)-1,2-*bis*(Benzyloxy)ethyl)-2,2-difluoropent-4-en-1-ol (10):** Weinreb amide **9a** (270 mg, 0.64 mmol) was dissolved in THF (10 mL). To the solution at 0 °C, $LiAlH_4$ (77 mg, 2.03 mmol) was added, and the resulting reaction mixture was stirred for 30 min. The reaction was quenched by adding water and 3 M aqueous NaOH. After the resultant mixture was diluted with $Et_2O$, $NaBH_4$ was added to it. The reaction mixture was stirred overnight, filtered, and purified by silica gel chromatography (1% MeOH in $CH_2Cl_2$) to give alcohol **10** (231 mg, 99%) as a clear oil. $^1$H NMR (400 MHz, $CDCl_3$): $\delta$ = 7.40–7.31 (m, 10H), 5.92 (dt, $J$ = 17.2, 10.0 Hz, 1H), 5.35–5.23 (m, 2H), 4.79–4.49 (m, 4H), 4.15–4.11 (m, 1H), 3.83–3.49 (m, 4H), 3.05–3.00 (m, 1H), 2.70 ppm (br, 1H); $^{13}$C NMR (100 MHz, $CDCl_3$): $\delta$ = 137.8, 130.0, 128.4, 127.9, 127.8, 127.7, 127.7, 122.6, 122.0, 75.7, 73.3, 73.0, 70.2, 63.3, 50.2 ppm: $^{19}$F NMR (376 MHz): $\delta$ = −109.61, −111.29 ppm; $[\alpha]_D^{23}$ = −17.9 ($c$ = 0.66, $CHCl_3$); LRMS (CI): 361 $[M-H]^+$.

**(*S*)-3-((*R*)-1,2-*bis*(Benzyloxy)ethyl)-2,2-difluoropent-4-en-1-ol (13):** Alcohol **13** was obtained as an oil in 96% yield from Weinreb amide **9b** through the same sequence of reactions as for alcohol **10**. $^1$H NMR (400 MHz, $CDCl_3$): $\delta$ = 7.40–7.32 (m, 10H), 5.78 (dt, $J$ = 17.4, 9.8 Hz, 1H), 5.36–5.29 (m, 2H), 4.83 (d, $J$ = 11.1 Hz, 1H), 4.60–4.52 (m, 3H), 3.96–3.61 (m, 5H), 3.23–3.10 (m, 1H), 3.00 ppm (br, 1H); $^{13}$C NMR (100 MHz, $CDCl_3$): $\delta$ = 138.0, 137.4, 130.4, 128.5, 128.4, 128.1, 128.0, 127.7, 122.8, 121.5, 77.2, 73.4, 72.8, 70.5, 63.9, 50.0 ppm; $^{19}$F NMR (376 MHz): $\delta$ = −104.01 ppm, −113.05; $[\alpha]_D^{23}$ = [+9.9 ($c$ = 1.06, $CHCl_3$); LRMS (CI): 363 $[M+H]^+$.

**(3*R*,3a*S*,6a*S*)-4,4-Difluorohexahydrofuro[2,3-*b*]furan-3-ol (12):** Alcohol **10** (231 mg, 0.63 mmol) was dissolved in $CH_2Cl_2$ (30 mL), and $O_3$ was bubbled through the solution for 5 min at −78 °C. After bubbling with argon, $PPh_3$ (510 mg, 1.94 mmol) was added to the solution. The resulting mixture was stirred for 2 h at −78 °C and then 3 h at 23 °C. The mixture was concentrated in vacuo, and the residue was passed through a silica gel column (hexanes/EtOAc, 4:1 to 2:1) to give crude lactol **11** (332 mg) as a clear oil.

The above crude lactol (332 mg) was then dissolved in EtOAc (25 mL), and palladium hydroxide (20% on activated carbon, 180 mg) was added to the solution. The resulting suspension was stirred under a hydrogen-filled balloon overnight. The reaction mixture was filtered through a pad of Celite, and the filtrate was evaporated in vacuo to give crude triol (150 mg) as a pale-yellow oil. This crude triol (150 mg) was dissolved in a mixture of $CH_2Cl_2$ and THF (30 mL and 5 mL), and camphorsulfonic acid (130 mg) was added to the solution. The reaction mixture was stirred overnight and neutralized with $NaHCO_3$ (100 mg). The resulting mixture was stirred for a further 4 h. After filtration and evaporation, the residue was purified by silica gel chromatography (1% MeOH in $CH_2Cl_2$) to provide the title difluoro-*bis*-THF ligand **12** (110 mg, 68% over three steps) as an amorphous solid. $^1$H NMR (400 MHz, $CDCl_3$): $\delta$ = 5.79 (d, $J$ = 5.3 Hz, 1H), 4.65–4.59 (m, 1H), 4.30–4.20 (m, 1H), 4.08–3.99 (m, 3H), 3.03–2.96 (m, 1H), 2.60 ppm (t, $J$ = 5.8 Hz, 1H); $^{13}$C NMR (100 MHz, $CDCl_3$): $\delta$ = 128.3, 108.3, 74.7, 72.9, 70.7, 51.8 ppm; $^{19}$F NMR (376 MHz): $\delta$ = −91.68 ppm, −122.38; $[\alpha]_D^{23}$ = +7.21 ($c$ = 0.68, $CHCl_3$); LRMS (CI): 167 $[M+H]^+$.

**(3*R*,3a*R*,6a*R*)-4,4-Difluorohexahydrofuro[2,3-*b*]furan-3-ol (14):** Difluoro-*bis*-THF **14** was obtained in 73% yield from alcohol **13** by following the same sequence of reactions as for compound **12**. $^1$H NMR (400 MHz, $CDCl_3$): $\delta$ = 6.00 (d, $J$ = 5.2 Hz, 1H), 4.66 (d, $J$ = 2.8 Hz, 1H), 4.07–3.88 (m, 4H), 3.09–3.02 (m, 1H), 2.69 ppm (br, 1H); $^{13}$C NMR (100 MHz, $CDCl_3$): $\delta$ = 126.7, 108.3, 76.3, 72.1, 71.9, 58.4 ppm; $^{19}$F NMR (376 MHz): $\delta$ = −97.60, −115.49 ppm; $[\alpha]_D^{23}$ = +10.8 ($c$ = 1.59, $CHCl_3$); LRMS (CI): 167 $[M+H]^+$.

**(3*S*,3a*R*,6a*R*)-4,4-Difluorohexahydrofuro[2,3-*b*]furan-3-ol (*ent*-12):** Difluoro alcohol **14** (38 mg, 0.23 mmol) was dissolved in $CH_2Cl_2$ (5 mL), and Dess–Martin periodinane (146 mg, 0.34 mmol) was added to the solution at 23 °C. Stirring was continued for 2 h. After this period, the reaction mixture was filtered through a short silica gel column using $CH_2Cl_2$ as the eluent to give crude ketone (35 mg). The crude ketone (35 mg) was dissolved in THF (4 mL), and the mixture was cooled to −78 °C. To the solution was added dropwise L-selectride (1 M in THF, 320 μL, 0.32 mmol), and the mixture was stirred for 30 min. The reaction was quenched with MeOH. After removing the solvent in vacuo, the residue was purified by silica gel chromatography (hexanes/EtOAc 3:1) to give difluoro-*bis*-THF ligand *ent*-**12** (32 mg, 84% over two steps) as an amorphous solid. $^1$H NMR (400 MHz, $CDCl_3$): $\delta$ = 5.79 (d, $J$ = 5.3 Hz, 1H), 4.65–4.59 (m, 1H), 4.30–4.20 (m, 1H), 4.08–3.99 (m, 3H), 3.03–2.96 (m, 1H), 2.60 ppm (t, $J$ = 5.8 Hz, 1H); $^{13}$C NMR (100 MHz, $CDCl_3$): $\delta$ = 128.3, 108.3, 74.7, 72.9, 70.7, 51.8 ppm; $^{19}$F NMR (376 MHz): $\delta$ = −91.68, −122.38 ppm; $[\alpha]_D^{23}$ = −7.9 ($c$ = 0.66, $CHCl_3$); LRMS (CI): 167 $[M+H]^+$.

**(3*R*,3a*S*,6a*S*)-4,4-Difluorohexahydrofuro[2,3-*b*]furan-3-yl (4-nitrophenyl)carbonate (15):** A solution of alcohol **12** (14.3 mg, 0.09 mmol) and pyridine (35 μL, 0.43 mmol) in $CH_2Cl_2$ (1 mL) was cooled to 0 °C, and 4-nitrophenyl chloroformate (54 mg, 0.26 mmol) was added to the solution in one portion. The reaction temperature was raised to 23 °C, and the mixture was stirred for 2 h. The reaction was quenched with EtOH, and the solvent was removed in vacuo. The residue was passed through a short silica gel column using hexanes/EtOAc 5:1 to 2:1 as the eluent to give carbonate **15** (25 mg).

Activated carbonate *ent*-**15** and **16** were prepared by following the procedure described for carbonate **15**. These unstable mixed activated carbonates were used directly for inhibitor synthesis.

**Inhibitor 3:** Activated mixed carbonate **15** (12.5 mg) was added to a solution of amine **17** (40 mg) and $Et_3N$ (150 μL) in $CH_2Cl_2$ (2 mL). The resulting reaction mixture was stirred for 3 days until all of the carbonate was consumed. After this period, solvents were evaporated, and the residue was purified by silica gel chromatography (1% MeOH in $CH_2Cl_2$) to give inhibitor **3** (18 mg, 83% for two steps from **12**). $^1$H NMR (400 MHz, $CDCl_3$): $\delta$ = 7.69 (d, $J$ = 8.8 Hz, 2H), 7.30–7.20 (m, 5H), 6.99–6.96 (m, 2H), 5.77 (d, $J$ = 5.1 Hz, 1H), 5.35–5.29 (m, 1H), 5.00 (d, $J$ = 8.3 Hz, 1H), 4.08–3.68 (m, 10H), 3.15–2.75 (m, 7H), 1.86–1.79 (m, 1H), 0.91–0.85 ppm (m, 6H); $^{13}$C NMR (100 MHz, $CDCl_3$): $\delta$ = 163.0, 154.8, 137.2, 129.7, 129.4, 128.5, 126.9, 126.5, 114.3, 108.1, 72.7, 72.3, 72.1, 71.1, 71.0, 58.7, 55.5, 55.1, 53.6, 50.1, 35.2, 27.2, 20.0, 19.8 ppm; $^{19}$F NMR (376 MHz): $\delta$ = −91.82, −123.21 ppm; LRMS (ESI): 599 $[M+H]^+$; HRMS-ESI ($m/z$): $[M+Na]^+$ calcd for $C_{28}H_{36}F_2N_2O_8SNa$: 621.2059, found: 621.2054.

**Inhibitor 4:** The title inhibitor was obtained in 58% yield from activated mixed carbonate **15** and amine **18** by following the same procedure as inhibitor **3**. $^1$H NMR (400 MHz, $CDCl_3$): $\delta$ = 7.53 (d, $J$ = 8.4 Hz, 2H), 7.32–7.21 (m, 5H), 6.68 (d, $J$ = 8.5 Hz, 2H), 5.78 (d, $J$ = 5.1 Hz, 1H), 5.35–5.28 (m, 1H), 4.76 (d, $J$ = 8.3 Hz, 1H), 4.23–3.70 (m, 9H), 3.15–2.72 (m, 7H), 1.86–1.73 (m, 1H), 0.93–0.87 ppm (m, 6H); $^{13}$C NMR (100 MHz, $CDCl_3$): $\delta$ = 154.8, 150.7, 137.2, 129.4, 128.5, 126.9, 126.5, 126.0, 114.0, 108.1, 72.7, 72.3, 72.1, 71.0, 58.8, 55.1, 53.7, 53.3, 50.1, 35.2, 27.2, 20.1, 19.8 ppm; $^{19}$F NMR (376 MHz): $\delta$ = −91.79, −123.24 ppm; LRMS (ESI): 584 $[M+H]^+$; HRMS-ESI ($m/z$): $[M+H]^+$ calcd for $C_{27}H_{36}F_2N_3O_7S$: 584.2242, found: 584.2245.

**Inhibitor 19:** The title inhibitor was obtained in 64% yield from activated mixed carbonate *ent*-**15** and amine **17** by following the same procedure as inhibitor **3**. $^1$H NMR (400 MHz, $CDCl_3$): $\delta$ = 7.71

(d, $J$=8.9 Hz, 2H), 7.32–7.22 (m, 5H), 6.97 (d, $J$=8.9 Hz, 2H), 5.77 (d, $J$=5.3 Hz, 1H), 5.29–5.25 (m, 1H), 4.93 (d, $J$=8.3 Hz, 1H), 4.12–3.75 (m, 10H), 3.19–2.70 (m, 7H), 1.83–1.71 (m, 1H), 0.92–0.84 ppm (m, 6H); $^{13}$C NMR (100 MHz, $CDCl_3$): $\delta$=163.0, 155.0, 137.2, 129.7, 129.4, 129.4, 128.5, 127.1, 126.6, 114.3, 108.1, 72.6, 72.4, 71.9, 71.1, 58.9, 55.5, 55.1, 53.7, 49.7, 35.7, 27.1, 20.0, 19.7 ppm; $^{19}$F NMR (376 MHz): $\delta$=−91.54, −123.41 ppm; LRMS (ESI): 599 $[M+H]^+$; HRMS-ESI ($m/z$): $[M+Na]^+$ calcd for $C_{28}H_{36}F_2N_2O_8SNa$: 621.2059, found: 621.2059.

**Inhibitor 20:** The title inhibitor was obtained in 64% yield from activated mixed carbonate **16** and amine **17** by following the same procedure as inhibitor **3**. $^1$H NMR (400 MHz, $CDCl_3$): $\delta$=7.70 (d, $J$=8.8 Hz, 2H), 7.31–7.22 (m, 5H), 6.99 (d, $J$=11.6 Hz, 2H), 5.87 (d, $J$=5.2 Hz, 1H), 5.24 (br, 1H), 4.98 (d, $J$=8.3 Hz, 1H), 4.04–3.69 (m, 10H), 3.17–2.75 (m, 7H), 1.88–1.77 (m, 1H), 0.93–0.87 ppm (m, 6H); $^{13}$C NMR (100 MHz, $CDCl_3$): $\delta$=164.0, 154.9, 137.3, 129.6, 129.4, 129.4, 128.5, 126.6, 126.3, 114.3, 108.1, 74.5, 73.9, 72.4, 72.0, 58.7, 55.7, 55.5, 55.0, 53.7, 35.5, 27.2, 20.0, 19.8 ppm; $^{19}$F NMR (376 MHz): $\delta$=−98.62, −114.71 ppm; LRMS (ESI): 599 $[M+H]^+$; HRMS-ESI ($m/z$): $[M+H]^+$ calcd for $C_{28}H_{37}F_2N_2O_8S$: 599.2238, found: 599.2227; HRMS-ESI ($m/z$): $[M+Na]^+$ calcd for $C_{28}H_{36}F_2N_2O_8SNa$: 621.2059, found: 621.2059.

**Inhibitor 21:** The title inhibitor was obtained in 70% yield from activated mixed carbonate **16** and amine **18** by following the same procedure as inhibitor **3**. $^1$H NMR (400 MHz, $CDCl_3$): $\delta$=7.53 (d, $J$=7.4 Hz, 2H), 7.32–7.21 (m, 5H), 6.68 (d, $J$=8.6 Hz, 2H), 5.87 (d, $J$=5.2 Hz, 1H), 5.24 (br, 1H), 4.94 (d, $J$=8.3 Hz, 1H), 4.22–3.68 (m, 9H), 3.17–2.74 (m, 7H), 1.85–1.76 (m, 1H), 0.93–0.86 ppm (m, 6H); $^{13}$C NMR (100 MHz, $CDCl_3$): $\delta$=154.9, 150.7, 137.4, 129.4, 128.4, 126.6, 126.3, 125.8, 114.0, 108.2, 74.5, 73.9, 72.4, 72.0, 58.8, 55.7, 55.0, 53.7, 35.5, 27.2, 20.1, 19.8 ppm; $^{19}$F NMR (376 MHz): $\delta$=−98.63, −114.70 ppm; LRMS (ESI): 584 $[M+H]^+$; HRMS-ESI ($m/z$): $[M+Na]^+$ calcd for $C_{27}H_{35}F_2N_3O_7SNa$: 606.2062, found: 606.2061.

**Determination of X-ray structures of HIV-1 protease–inhibitor 4 complexes:** The optimized HIV-1 protease was expressed and purified as described.[31] The protease–inhibitor complex was crystallized by the hanging-drop vapor-diffusion method with well solutions of 1.0 M NaCl, 0.1 M sodium acetate buffer (pH 4.8). Diffraction data were collected on a single crystal cooled to 90 K at the SER-CAT (22-BM beamline), Advanced Photon Source, Argonne National Lab (Chicago, IL, USA) with X-ray wavelength of 1.0 Å, and processed by HKL-2000[32] with an $R_{merge}$ of 6.2%. Using the isomorphous structure,[33] the crystal structure was solved by PHASER[34] in the CCP4i Suite[35,36] and refined by SHELX-97[37,38] with 1.3 Å resolution data. COOT[39] was used for manual modification of the atomic structure. PRODRG-2[40] was used to construct the inhibitor and the restraints for refinement. Alternative conformations were modeled, anisotropic atomic displacement parameters ($B$ factors) were applied for all atoms including solvent molecules, and hydrogen atoms were added in the final round of refinement. The final refined solvent structure included one $Na^+$ ion, three $Cl^-$ ions, two acetate and 129 water molecules. The crystallographic statistics are listed in Table S1, Supporting Information. The coordinates and structure factors of the protease in complex with GRL-05010A have been deposited in the RCSB Protein Data Bank[41] with PDB ID: 4U8W.

## Acknowledgements

*This research was supported by grants from the US National Institutes of Health (GM53386 to A.K.G., and GM62920 to I.T.W.). This work was also supported by the Intramural Research Program of the Center for Cancer Research, US National Cancer Institute, National Institutes of Health, and in part by a Grant-in-aid for Scientific Research (Priority Areas) from the Ministry of Education, Culture, Sports, Science, and Technology of Japan (Monbu-Kagakusho), a Grant for Promotion of AIDS Research from the Ministry of Health, Welfare, and Labor of Japan (Kosei Rohdosho: H15-AIDS-001), and the Grant to the Cooperative Research Project on Clinical and Epidemiological Studies of Emerging and Reemerging Infectious Diseases (Kumamoto University) of Monbu-Kagakusho. The authors also thank Ms. Heather Osswald (Purdue University) for helpful discussions.*

**Keywords:** antiviral agents · blood–brain barrier · HIV-1 protease · inhibitors · ligands · multidrug resistance

[1] S. Purser, P. R. Moore, S. Swallow, V. Gouverneur, *Chem. Soc. Rev.* **2008**, *37*, 320–330.
[2] H. J. Böhm, D. Banner, S. Bendels, M. Kansy, B. Kuhn, K. Müller, U. Obst-Sander, M. Stahl, *ChemBioChem* **2004**, *5*, 637–643.
[3] B. K. Park, N. R. Kitteringham, P. M. O'Neill, *Annu. Rev. Pharmacol. Toxicol.* **2001**, *41*, 443–470.
[4] B. E. Smart, *J. Fluorine Chem.* **2001**, *109*, 3–11.
[5] A. K. Ghosh, D. D. Anderson, I. T. Weber, H. Mitsuya, *Angew. Chem. Int. Ed.* **2012**, *51*, 1778–1802; *Angew. Chem.* **2012**, *124*, 1812–1838.
[6] A. K. Ghosh, B. D. Chapsal, I. T. Weber, H. Mitsuya, *Acc. Chem. Res.* **2008**, *41*, 78–86.
[7] A. K. Ghosh, J. F. Kincaid, W. Cho, D. E. Walters, K. Krishnan, K. A. Hussain, Y. Koo, H. Cho, C. Rudall, L. Holland, J. Buthod, *Bioorg. Med. Chem. Lett.* **1998**, *8*, 687–690.
[8] Y. Koh, H. Nakata, K. Maeda, H. Ogata, G. Bilcer, T. Devasamudram, J. F. Kincaid, P. Boross, Y. F. Wang, Y. Tie, P. Volarath, L. Gaddis, R. W. Harrison, I. T. Weber, A. K. Ghosh, H. Mitsuya, *Antimicrob. Agents Chemother.* **2003**, *47*, 3123–3129.
[9] A. K. Ghosh, Z. L. Dawson, H. Mitsuya, *Bioorg. Med. Chem.* **2007**, *15*, 7576–7580.
[10] A. K. Ghosh, P. R. Sridhar, N. Kumaragurubaran, Y. Koh, I. T. Weber, H. Mitsuya, *ChemMedChem* **2006**, *1*, 939–950.
[11] A. K. Ghosh, C. D. Martyr in *Modern Drug Synthesis* (Eds.: J. J. Li, D. S. Johnson), Wiley, Hoboken, **2010**, pp. 29–44.
[12] Y. Tie, P. I. Boross, Y.-F. Wang, L. Gaddis, A. K. Hussain, S. Leshchenko, A. K. Ghosh, J. M. Louis, R. W. Harrison, I. T. Weber, *J. Mol. Biol.* **2004**, *338*, 341–352.
[13] J. C. McArthur, B. J. Brew, A. Nath, *Lancet Neurol.* **2005**, *4*, 543–555.
[14] S. Kramer-Hämmerle, I. Rothenaigner, H. Wolff, J. E. Bell, R. Brack-Werner, *Virus Res.* **2005**, *111*, 194–213.
[15] I. L. Tan, J. C. McArthur, *CNS Drugs* **2012**, *26*, 123–134.
[16] D. Langford, J. Marquie-Beck, S. de Almeida, D. Lazzaretto, S. Letendre, I. Grant, J. A. McCutchan, E. Masliah, R. J. Ellis, *J. Neurovirol.* **2006**, *12*, 100–107.
[17] A. Vulpetti, N. Schiering, C. Dalvit, *Proteins Struct. Funct. Bioinf.* **2010**, *78*, 3281–3291.
[18] P. Zhou, J. Zou, F. Tian, Z. Shang, *J. Chem. Inf. Model.* **2009**, *49*, 2344–2355.
[19] K. Fujita, H. Nakai, S. Kobayashi, K. Inoue, S. Nojima, M. Ohno, *Tetrahedron Lett.* **1982**, *23*, 3507–3510.
[20] Y. Y. Yang, J. Xu, Z. W. You, X. H. Xu, X. L. Qiu, F. L. Qing, *Org. Lett.* **2007**, *9*, 5437–5440.
[21] Y. Y. Yang, W. D. Meng, F. L. Qing, *Org. Lett.* **2004**, *6*, 4257–4259.
[22] H. Greuter, R. W. Lang, A. J. Romann, *Tetrahedron Lett.* **1988**, *29*, 3291–3294.
[23] A. K. Ghosh, B. D. Chapsal, G. L. Parham, M. Steffey, J. Agniswamy, Y.-F. Wang, M. Amano, I. T. Weber, H. Mitsuya, *J. Med. Chem.* **2011**, *54*, 5890–5901.
[24] A. K. Ghosh, S. Leshchenko, M. Noetzel, *J. Org. Chem.* **2004**, *69*, 7822–7829.

[25] M. V. Toth, G. R. Marshall, *Int. J. Pept. Protein Res.* **1990**, *36*, 544–550.
[26] M. Amano, Y. Koh, D. Das, J. Li, S. Leschenko, Y. F. Wang, P. I. Boross, I. T. Weber, A. K. Ghosh, H. Mitsuya, *Antimicrob. Agents Chemother.* **2007**, *51*, 2143–2155.
[27] K. Yoshimura, R. Kato, M. F. Kavlick, A. Nguyen, V. Maroun, K. Maeda, K. A. Hussain, A. K. Ghosh, S. V. Gulnik, J. W. Erickson, H. Mitsuya, *J. Virol.* **2002**, *76*, 1349–1358.
[28] P. M. Salcedo Gomez, M. Amano, S. Yashchuk, A. Mizuno, D. Das, A. K. Ghosh, H. Mitsuya, *Antimicrob. Agents Chemother.* **2013**, *57*, 6110–6121.
[29] S. Nakagawa, M. A. Deli, S. Nakao, M. Honda, K. Hayashi, R. Nakaoke, Y. Kataoka, M. Niwa, *Cell. Mol. Neurobiol.* **2007**, *27*, 687–694.
[30] R. Cecchelli, V. Berezowski, S. Lundquist, M. Culot, M. Renftel, M. P. Dehouck, L. Fenart, *Nat. Rev. Drug Discovery* **2007**, *6*, 650–661.
[31] B. Mahalingam, J. M. Louis, J. Hung, R. W. Harrison, I. T. Weber, *Proteins* **2001**, *43*, 455–464.
[32] *"Processing of X-Ray Diffraction Data Collected in Oscillation Mode", Z. Otwinowski, W. Minor in Methods in Enzymology: Macromolecular Crystallography, Part A, Vol. 276* (Eds.: C. W. Carter, Jr. and R. M. Sweet), Academic Press, New York, **1997**, pp. 307–326.
[33] Y. F. Wang, Y. Tie, P. I. Boross, J. Tozser, A. K. Ghosh, R. W. Harrison, I. T. Weber, *J. Med. Chem.* **2007**, *50*, 4509–4515.
[34] A. J. McCoy, R. W. Grosse-Kunstleve, P. D. Adams, M. D. Winn, L. C. Storoni, R. J. Read, *J. Appl. Crystallogr.* **2007**, *40*, 658–674.
[35] Collaborative Computational Project Number 4, The CCP4 Suite: Programs for Protein Crystallography, *Acta Crystallogr. Sect. D* **1994**, *50*, 760–763.
[36] E. Potterton, P. Briggs, M. Turkenburg, E. Dodson, *Acta Crystallogr. Sect. D* **2003**, *59*, 1131–1137.
[37] G. M. Sheldrick, *Acta Crystallogr. Sect. A* **2008**, *64*, 112–122.
[38] G. M. Sheldrick, T. R. Schneider, *Methods Enzymol.* **1997**, *277*, 319–343.
[39] P. Emsley, K. Cowtan, *Acta Crystallogr. Sect. D* **2004**, *60*, 2126–2132.
[40] A. W. Schüttelkopf, D. M. F. van Aalten, *Acta Crystallogr. Sect. D* **2004**, *60*, 1355–1363.
[41] H. M. Berman, J. Westbrook, Z. Feng, G. Gilliland, T. N. Bhat, H. Weissig, I. N. Shindyalov, P. E. Bourne, *Nucleic Acids Res.* **2000**, *28*, 235–242.

Received: August 18, 2014
Published online on October 21, 2014

AAC
Journals.ASM.org

# A Conserved Hydrogen-Bonding Network of P2 *bis*-Tetrahydrofuran-Containing HIV-1 Protease Inhibitors (PIs) with a Protease Active-Site Amino Acid Backbone Aids in Their Activity against PI-Resistant HIV

Ravikiran S. Yedidi,[a] Harisha Garimella,[a] Manabu Aoki,[b,c] Hiromi Aoki-Ogata,[b] Darshan V. Desai,[a] Simon B. Chang,[a] David A. Davis,[d] W. Sean Fyvie,[e] Joshua D. Kaufman,[f] David W. Smith,[g] Debananda Das,[a] Paul T. Wingfield,[f] Kenji Maeda,[a] Arun K. Ghosh,[e] Hiroaki Mitsuya[a,b]

Experimental Retrovirology Section[a] and Retroviral Disease Section,[d] HIV and AIDS Malignancy Branch, National Cancer Institute, National Institutes of Health, Bethesda, Maryland, USA; Departments of Hematology and Infectious Diseases, Kumamoto University Graduate School of Biomedical Sciences, Kumamoto, Japan[b]; Department of Medical Technology, Kumamoto Health Science University, Kumamoto, Japan[c]; Departments of Chemistry and Medicinal Chemistry, Purdue University, West Lafayette, Indiana, USA[e]; Protein Expression Laboratory, National Institute of Arthritis and Musculoskeletal and Skin Diseases, National Institutes of Health, Bethesda, Maryland, USA[f]; Life Sciences Collaborative Access Team, Synchrotron Research Center, Northwestern University, Argonne, Illinois, USA[g]

**In the present study, GRL008, a novel nonpeptidic human immunodeficiency virus type 1 (HIV-1) protease inhibitor (PI), and darunavir (DRV), both of which contain a P2-*bis*-tetrahydrofuranyl urethane (*bis*-THF) moiety, were found to exert potent antiviral activity (50% effective concentrations [$EC_{50}$s], 0.029 and 0.002 μM, respectively) against a multidrug-resistant clinical isolate of HIV-1 ($HIV_{A02}$) compared to ritonavir (RTV; $EC_{50}$, >1.0 μM) and tipranavir (TPV; $EC_{50}$, 0.364 μM). Additionally, GRL008 showed potent antiviral activity against an HIV-1 variant selected in the presence of DRV over 20 passages ($HIV_{DRV^{R}P20}$), with a 2.6-fold increase in its $EC_{50}$ (0.097 μM) compared to its corresponding $EC_{50}$ (0.038 μM) against wild-type HIV-$1_{NL4-3}$ ($HIV_{WT}$). Based on X-ray crystallographic analysis, both GRL008 and DRV showed strong hydrogen bonds (H-bonds) with the backbone-amide nitrogen/carbonyl oxygen atoms of conserved active-site amino acids G27, D29, D30, and D30′ of $HIV_{A02}$ protease ($PR_{A02}$) and wild-type PR in their corresponding crystal structures, while TPV lacked H-bonds with G27 and D30′ due to an absence of polar groups. The P2′ thiazolyl moiety of RTV showed two conformations in the crystal structure of the $PR_{A02}$-RTV complex, one of which showed loss of contacts in the S2′ binding pocket of $PR_{A02}$, supporting RTV's compromised antiviral activity ($EC_{50}$, >1 μM). Thus, the conserved H-bonding network of P2-*bis*-THF-containing GRL008 with the backbone of G27, D29, D30, and D30′ most likely contributes to its persistently greater antiviral activity against $HIV_{WT}$, $HIV_{A02}$, and $HIV_{DRV^{R}P20}$.**

Human immunodeficiency virus type 1 (HIV-1) protease (PR) is a critical viral component that is required for viral maturation and infectivity (1, 2). Due to rapid and error-prone viral replication, drug-resistant HIV-1 variants are inevitably selected during therapy with all currently available antiretroviral agents (3). Accumulation of mutations in the protease-encoding gene results in the emergence of multidrug-resistant (MDR) HIV-1 variants carrying a protease with an altered three-dimensional structure (4). Darunavir (DRV) (Fig. 1), the latest FDA-approved protease inhibitor (PI), which contains *bis*-tetrahydrofuranyl urethane (*bis*-THF) as the P2 moiety, has been shown to have a high genetic barrier (5, 6), a feature of a drug or regimen that delays or prevents the occurrence of genetic evolution of HIV-1 to acquire drug resistance-associated mutations, allowing the virus to overcome the antiretroviral activity of the very drug or regimen and to become capable of propagating despite treatment with the very drug or regimen. However, HIV-1 also ultimately develops high levels of resistance to DRV both *in vitro* and *in vivo* (7, 8). In order to suppress the propagation of such PI-resistant HIV-1 protease variants, the development of novel PIs with greater antiviral activities and higher genetic barriers is urgently needed.

Previously, two structurally related nonpeptidic PIs, GRL007 and GRL008, were designed based on the crystal structure of wild type HIV-1 protease ($PR_{WT}$) in complex with DRV (PDB ID 4HLA) to replace one of the crystallographic bridging water molecules seen between the P2′ aniline moiety of DRV and G48′ of $PR_{WT}$ (9). Both GRL007 and GRL008 contain *bis*-THF as the P2 moiety, while the former has benzene carboxylic acid and the latter has benzene carboxamide as the P2′ moiety. Both compounds were evaluated against wild-type HIV-1 ($HIV_{WT}$) (9). While both GRL007 and GRL008 showed greater enzyme inhibitory activities than the parent compound (DRV), GRL007 failed to inhibit the replication of $HIV_{WT}$ at up to 1 μM due to its poor cell penetration capability. On the other hand, GRL008 achieved higher intracellular concentrations as DRV comparably did and showed favorable antiviral activity against $HIV_{WT}$ (9).

In the present study, GRL008 (Fig. 1) was evaluated against an MDR clinical isolate of HIV-1 ($HIV_{A02}$) (10, 11) that contained eight amino acid substitutions, L10I, K45R, I54V, L63P, A71V, V82T, L90M, and I93L, in its protease ($PR_{A02}$). The antiviral activity of GRL008 was also evaluated against HIV-$2_{ROD}$ and an

Received 16 January 2014 Returned for modification 10 February 2014
Accepted 25 March 2014
Published ahead of print 21 April 2014
Address correspondence to Hiroaki Mitsuya, mitsuyah@helix.nih.gov.
Supplemental material for this article may be found at http://dx.doi.org/10.1128/AAC.00107-14.

doi:10.1128/AAC.00107-14

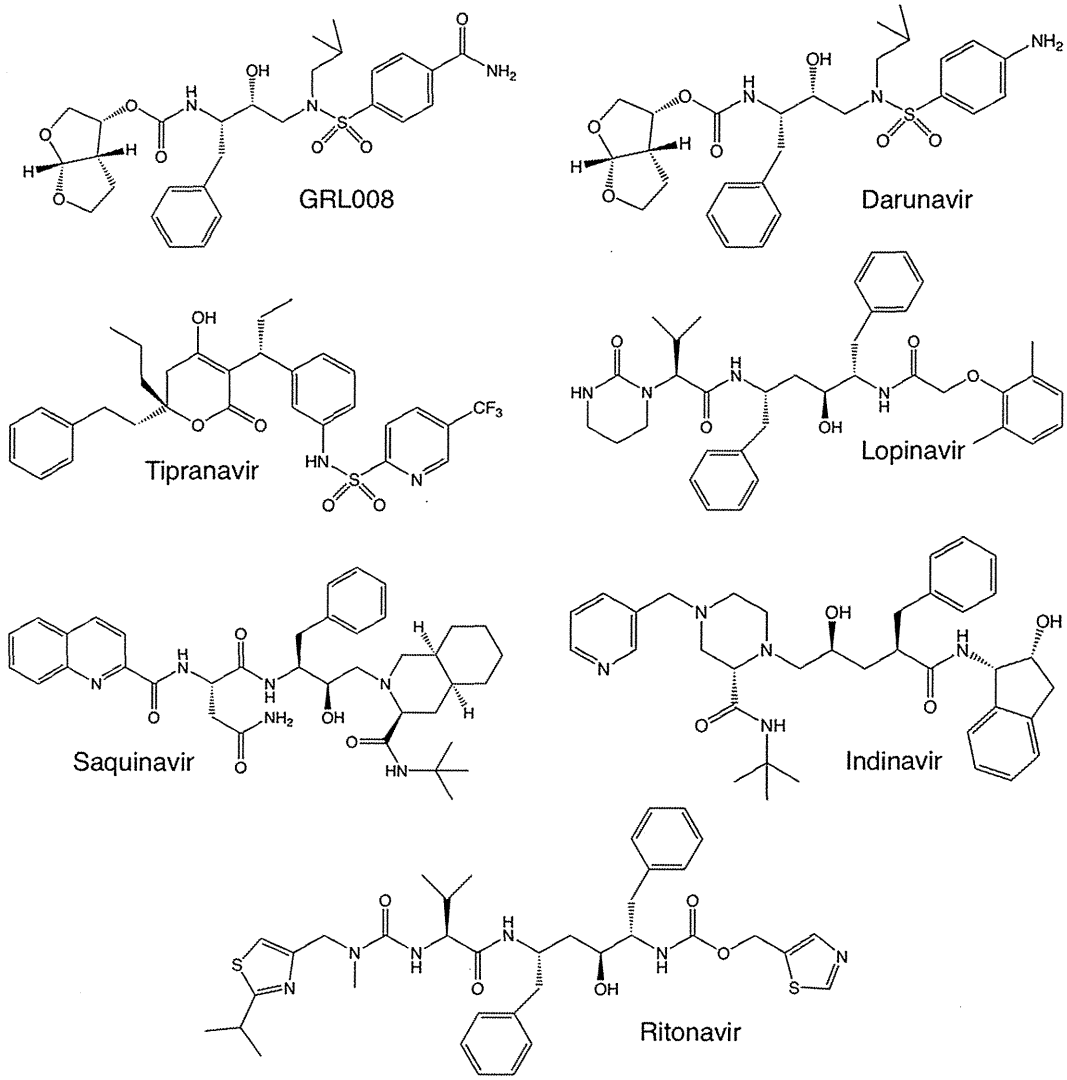


FIG 1 Structures of protease inhibitors used in this study. GRL008 is a novel experimental HIV-1 PI, while DRV, tipranavir, lopinavir, saquinavir, indinavir, and ritonavir are FDA-approved PIs. Both GRL008 and DRV contain *bis*-THF as the P2 moiety. GRL008 and DRV contain benzene carboxamide and aniline, respectively, as the P2′ moieties.

HIV-1 variant selected with DRV over 20 passages ($HIV_{DRV^{R}P20}$) (7). In addition, GRL008, DRV, ritonavir (RTV), and tipranavir (TPV) were individually cocrystallized with $PR_{A02}$, and a structure-function evaluation of each agent was performed. Crystal structures of $PR_{WT}$ in complex with GRL008, DRV, RTV, and TPV were published previously, with the following Protein Data Bank (PDB) identification codes: 4I8Z, 4HLA, 1HXW, and 2O4P, respectively.

## MATERIALS AND METHODS

**Protease inhibitors.** Indinavir (IDV), lopinavir (LPV), RTV, saquinavir (SQV), and TPV were provided by the NIH AIDS Research and Reference Reagent Program. DRV was synthesized as described previously (12). GRL008 was synthesized by Arun K. Ghosh and coworkers (details of the synthetic procedures will be published separately).

**Antiviral assays.** Antiviral assays were performed as described previously (9). Briefly, human MT-4 cells were cultured in RPMI 1640 (supplemented with 10% fetal bovine serum) and were exposed to $HIV_{WT}$ ($HIV\text{-}1_{NL4-3}$), $HIV_{A02}$, $HIV\text{-}2_{ROD}$, or $HIV_{DRV^{R}P20}$ in the presence of various concentrations (1 μM, 100 nM, 10 nM, and 1 nM) of the PIs. Fifty $TCID_{50}$ doses (the $TCID_{50}$ is the inoculum size of HIV-1 that causes a cytopathic effect in 50% of the target cells, i.e., the 50% tissue culture infective dose) were used to infect the MT-4 cells. Infected cells were cultured for 5 days in the presence of PIs. An MTT (3-[4,5-dimethylthiazol-2yl]-2,5-diphenyl tetrazolium bromide)-based colorimetric assay was performed to assess cell viability on day 5. Assays were conducted in triplicate. The antiviral data are summarized in Table 1.

**Expression and purification of $PR_{A02}$.** Expression and purification of $PR_{A02}$ was performed as described previously (9). Briefly, the inclusion bodies containing $PR_{A02}$ were extracted with 3 M guanidine HCl (GnCl), the mixture was centrifuged, and the supernatant was loaded on a Sephadex 200 column that was preequilibrated with 4 M GnCl. Protease-containing fractions were pooled and further purified by using a reverse-phase column. Fractions were analyzed by sodium dodecyl sulfate-polyacrylamide gel electrophoresis (SDS-PAGE), and the purity of $PR_{A02}$ was determined to be >95%.

**Protease refolding and cocrystallization with PIs.** Protease refolding was performed as described previously (9). Briefly, lyophilized $PR_{A02}$ was

TABLE 1 Anti-HIV[a] activity of GRL008 in comparison with activities of FDA-approved protease inhibitors

| PI | Mean $EC_{50}$ (μM) ± SD (fold change)[b] | | | |
|---|---|---|---|---|
| | HIV-$1_{NL4-3}$[c] | HIV-$2_{ROD}$ | HIV-$1_{A02}$ | HIV-$1_{DRV^{R}P20}$ |
| GRL008 | 0.038 ± 0.01 | 0.03 ± 0.006 | 0.029 ± 0.001 (0.8) | 0.097 ± 0.028 (2.6) |
| DRV | 0.001 ± 0.001 | 0.0057 ± 0.0028 | 0.002 ± 0.001 (2.0) | 0.05 ± 0.004 (50) |
| TPV | 0.128 ± 0.09 | 1.8 ± 0.3 | 0.364 ± 0.14 (2.8) | 0.34 ± 0.03 (2.7) |
| LPV | 0.029 ± 0.01 | 0.014 ± 0.002 | 0.474 ± 0.22 (16.3) | >1 (>34.0) |
| IDV | 0.039 ± 0.02 | ND | 0.526 ± 0.15 (13.5) | ND |
| RTV | 0.034 ± 0.02 | 0.26 ± 0.03 | >1 (>29.0) | >1 (>29.0) |
| SQV | 0.017 ± 0.01 | ND | 0.107 ± 0.08 (6.3) | ND |

[a] The amino acid substitutions identified in the proteases of HIV-$1_{A02}$ and HIV-$1_{DRV^{R}P20}$ compared to the wild-type HIV-$1_{NL4-3}$ were as follows: L10I/K45R/I54V/L63P/A71V/V82T/L90 M/I93L and L10I/I15V/K20R/L24I/V32I/M36I/M46L/L63P/A71T/V82A/L89M, respectively.

[b] The fold change is the ratio of the $EC_{50}$ of the inhibitor against HIV-$1_{A02}$ or HIV-$1_{DRV^{R}P20}$ and the corresponding $EC_{50}$ against HIV-$1_{NL4-3}$. ND, not determined.

[c] The $EC_{50}$s of GRL008, TPV, and SQV against wild-type HIV-1 (HIV-$1_{NL4-3}$) were obtained from data previously published (9).

dissolved in 1 ml of a 50% acetic acid solution and then added dropwise to 29 ml of refolding buffer (50 mM sodium acetate [pH 5.2], 5% ethylene glycol, 10% glycerol, 5 mM dithiothreitol, and a 10- to 20-fold molar excess of PI) while stirring on ice. Refolding was continued at 4°C with constant stirring overnight. The refolded protease-drug complex was concentrated using Amicon filters (3-kDa molecular mass cutoff) by centrifugation at 4,000 × *g*. The final protease concentration was determined to be 2 mg/ml. The hanging drop vapor diffusion method was used for cocrystallization of $PR_{A02}$-drug complexes. Two microliters of the $PR_{A02}$-drug complex was mixed with 2 μl of well solution per drop. Ammonium sulfate and sodium chloride grid screens (Hampton Research, CA) were used to obtain preliminary crystallization hits. Crystals were usually obtained in 1 to 2 days at room temperature (298 K). Cocrystals of $PR_{A02}$ in complex with GRL008, DRV, TPV, or RTV were obtained using 1.6 M ammonium sulfate (in 0.1 M citric acid buffer at pH 5.0), 1 M sodium chloride (in 0.1 M citric acid buffer at pH 5.0), 2.4 M ammonium sulfate (in 0.1 M HEPES buffer at pH 7.0), and 3 M sodium chloride (in 0.1 M HEPES buffer at pH 7.0), respectively. Cocrystals were obtained as clusters of plates that were carefully dissociated using microtools, and individual crystals were picked up into nylon loops. Glucose (30%) was used as cryoprotectant for all the cocrystals. Cryo-coated cocrystals were instantaneously frozen in liquid nitrogen.

**X-ray diffraction data collection and processing details.** X-ray diffraction data were collected at the Advanced Photon Source (APS), Argonne National Laboratory IL. Diffraction data for $PR_{A02}$-GRL008 and $PR_{A02}$-RTV were collected at the SER-CAT (Southeast Regional Collaborative Access Team) facility, beam line 22-ID (insertion device; wavelength, 1.0 Å) equipped with a Mar300 charge-coupled-device (CCD) detector. Diffraction data for $PR_{A02}$-TPV were collected at the LS-CAT (Life Sciences Collaborative Access Team) facility, beam line 21-ID (wavelength, 0.98 Å) equipped with an MX225 CCD detector, while the diffraction data for $PR_{A02}$-DRV were collected using a Rigaku 007 HF rotating anode X-ray generator (Cu $K_{\alpha}$ wavelength, 1.54 Å) equipped with multilayer focusing mirrors and a Saturn A200 CCD detector. Sample temperature, crystal to detector distance, and frame width were 100 K, 200 mm, and 1°, respectively, at the synchrotron, while they were 95 K, 100 mm, and 0.5°, respectively, on the Rigaku generator. Diffraction data for $PR_{A02}$-GRL008 and $PR_{A02}$-RTV were processed and scaled using HKL2000 (13); data for $PR_{A02}$-TPV and $PR_{A02}$-DRV were processed using *i*MOSFLM (14) and scaled using SCALA (15) through the CCP4 interface (16, 17). Details of diffraction data processing results are given in Table 2.

**Structure solutions and refinement.** Structure solutions were obtained by the molecular replacement (MR) method. Initial MR was performed using MOLREP (18) through the CCP4 interface for $PR_{A02}$ with the protease taken from PDB ID 4HLA as a search model. Amino acid substitutions were modeled into 4HLA by using Maestro (version 9.3; Schrödinger, LLC, New York, NY). Final MR solution of $PR_{A02}$ was obtained using BALBES (19), an automated molecular replacement pipeline available from the York Structural Biology Laboratory server (http://www.york.ac.uk/chemistry/research/ysbl). Structure solutions were directly refined using REFMAC5 (20) through the CCP4 interface. Initial coordinates for GRL008, DRV, RTV, and TPV were taken from crystal structures (PDB IDs 4I8Z, 4HLA, 1HXW, and 2O4P, respectively). The PIs were fit into the electron density by using ARP/wARP ligands (21, 22) through the CCP4 interface. Refinement libraries for GRL008 were prepared using the PRODRG server (23) as described previously (9). Solvent molecules were built using the ARP/wARP solvent-building module through the CCP4 interface. After building water molecules, the final models were refined using the simulated annealing method from phenix.refine (Phenix, version 1.8.2-1309) (24) on the NIH Biowulf Linux cluster. Details of the refinement statistics are given in Table 2. The final refined structures were used for structural analysis. Hydrogen bonds (H-bonds) were calculated by using cutoff values for distance (maximum distance between the donor and acceptor heavy atoms was 3.0 Å) and angles (minimum donor, 90°, and minimum acceptor, 60°). H-bonds with a distance of >3.0 Å were considered as weak interactions. Hydrophobic contacts were calculated between two carbon atoms (one from PI and one from $PR_{WT}$ or $PR_{A02}$) with a 4-Å distance cutoff.

**Protein structure accession numbers.** The final refined coordinates for the crystal structures of $PR_{A02}$-GRL008, $PR_{A02}$-DRV, $PR_{A02}$-TPV, and $PR_{A02}$-RTV were deposited in the Research Collaboratory for Structural Bioinformatics Protein Data Bank (RCSB PDB) under accession IDs 4NJS, 4NJT, 4NJU, and 4NJV, respectively.

## RESULTS

**GRL008 is highly active against $HIV_{A02}$.** Cell-based antiviral assays using human MT-4 cells exposed to $HIV_{A02}$ revealed that GRL008 is highly active against $HIV_{A02}$, with an $EC_{50}$ of 0.029 μM. GRL008 and DRV, both of which contain a P2 *bis*-THF moiety, had <1- and 2-fold changes in their $EC_{50}$s against $HIV_{A02}$ compared to their corresponding $EC_{50}$s against $HIV_{WT}$ (Table 1). In contrast, as shown in Table 1, the $EC_{50}$s of RTV against $HIV_{WT}$ and $HIV_{A02}$ were 0.034 μM and >1 μM, respectively, resulting in a >29-fold increase in the $EC_{50}$ against $HIV_{A02}$. Similarly, LPV and IDV showed >16- and >13-fold increases in their $EC_{50}$s, respectively, against $HIV_{A02}$ in comparison to their corresponding $EC_{50}$s against $HIV_{WT}$. Although lesser changes in the $EC_{50}$s were seen for IDV than for LPV, the $EC_{50}$ of IDV (0.526 μM) was still greater than that of LPV (0.474 μM) against $HIV_{A02}$. TPV and SQV showed 2.8- and >6-fold changes, respectively, in their $EC_{50}$s against $HIV_{A02}$ compared to their corresponding $EC_{50}$s against $HIV_{WT}$. However, SQV had greater antiviral potency against $HIV_{A02}$ ($EC_{50}$, 0.107 μM) than TPV ($EC_{50}$, 0.364 μM). Among the seven PIs tested, based on their antiviral activities,

TABLE 2 X-ray diffraction data and structure refinement details for $PR_{A02}$ in complex with GRL008, DRV, TPV, or RTV

| Parameter | $PR_{A02}$-GRL008 | $PR_{A02}$-DRV | $PR_{A02}$-TPV | $PR_{A02}$-RTV |
|---|---|---|---|---|
| PDB entry | 4NJS | 4NJT | 4NJU | 4NJV |
| Diffraction data | | | | |
| Resolution range (Å) | 35.37–1.80 | 28.83–1.95 | 34.62–1.80 | 34.81–1.80 |
| Unit cell | | | | |
| a (Å) | 44.632 | 44.95 | 45.35 | 45.952 |
| b (Å) | 57.995 | 57.60 | 57.54 | 58.219 |
| c (Å) | 88.111 | 86.48 | 86.70 | 86.866 |
| α (°) | 90.000 | 90.000 | 90.000 | 90.000 |
| β (°) | 90.030 | 90.020 | 90.020 | 90.020 |
| γ (°) | 90.000 | 90.000 | 90.000 | 90.000 |
| Space group | $P2_1$ | $P2_1$ | $P2_1$ | $P2_1$ |
| Solvent content (%) | 53.34 | 52.27 | 52.96 | 54.02 |
| No. of unique reflections | 41,155 (1,909)[a] | 31,996 (4,519) | 41,189 (5,915) | 40,844 (1,408) |
| Mean [I/σ(I)] | 23.1 (1.9) | 7.6 (2.1) | 10.1 (2.9) | 18.71 (1.8) |
| $R_{merge}$[b] | 0.090 (0.478) | 0.097 (0.472) | 0.089 (0.456) | 0.089 (0.398) |
| Data redundancy | 3.8 (2.2) | 3.2 (2.8) | 4.2 (4.1) | 3.4 (2.1) |
| Completeness (%) | 98.9 (92.3) | 98.5 (95.7) | 99.1 (98.6) | 96.6 (67.0) |
| Structure refinement data | | | | |
| Resolution range (Å) | 35.37–1.80 | 22.47–1.95 | 34.62–1.80 | 34.81–1.80 |
| No. of reflections used | 40,957 | 31,875 | 41,166 | 40,761 |
| $R_{cryst}$[c] | 0.1823 | 0.1996 | 0.1840 | 0.1868 |
| $R_{free}$[d] | 0.2161 | 0.2425 | 0.2211 | 0.2160 |
| No. of $PR_{A02}$ dimers/AU | 2 | 2 | 2 | 2 |
| No. of protein atoms/AU | 3,044 | 3,064 | 3,044 | 3,064 |
| No. of ligand molecules/AU | 2 | 2 | 2 | 4 |
| No. of ligand atoms/AU | 80 | 76 | 84 | 200 |
| No. of water molecules | 378 | 420 | 375 | 359 |
| Mean temp factors | | | | |
| Protein (Å$^2$) | 22.538 | 18.339 | 20.142 | 21.705 |
| Main chains (Å$^2$) | 20.390 | 16.818 | 17.930 | 19.213 |
| Side chains (Å$^2$) | 24.870 | 19.966 | 22.542 | 24.373 |
| Ligand (Å$^2$) | 17.672 | 15.725 | 16.28 | 22.574 |
| Water molecules (Å$^2$) | 32.114 | 26.305 | 30.263 | 31.957 |
| RMSD bond length (Å) | 0.007 | 0.009 | 0.007 | 0.009 |
| RMSD bond angle (Å) | 1.160 | 1.261 | 1.185 | 1.279 |
| Ramachandran plot | | | | |
| Most favored (%) | 97.8 | 96.5 | 98.1 | 97.8 |
| Additional allowed (%) | 1.9 | 3.5 | 1.9 | 2.2 |
| Generously allowed (%) | 0.3 | 0.0 | 0.0 | 0.0 |
| Disallowed (%) | 0.0 | 0.0 | 0.0 | 0.0 |

[a] Values in parentheses are for the highest-resolution shell.
[b] $R_{merge} = \Sigma|I - <I>|/\Sigma I$.
[c] $R_{cryst} = \Sigma ||F_{obs}| - |F_{calc}||/\Sigma|F_{obs}|$.
[d] A test set of 5% of the reflections was used for the $R_{free}$ analysis.

RTV, LPV, IDV, and TPV were the least effective against $HIV_{A02}$, all with $EC_{50}$s in the high nanomolar concentration range (364 nM to >1,000 nM). The substantial changes in the $EC_{50}$s for these drugs demonstrate the multidrug resistance profile of $HIV_{A02}$. Comparative analysis of the $EC_{50}$s against $HIV_{A02}$ given in Table 1 shows that the antiviral potency of GRL008 is >34-fold higher than RTV, >16-fold higher than LPV, >18-fold higher than IDV, 3.7-fold higher than SQV, and >12-fold higher than TPV. These results suggest that GRL008 has a desirable genetic barrier similar to that of DRV and can effectively inhibit multi-PI-resistant strains of HIV-1, such as $HIV_{A02}$.

**GRL008 shows favorable antiviral activities against HIV-$2_{ROD}$ and $HIV_{DRV}{}^{R}{}_{P20}$.** The favorable antiviral activity of GRL008 against $HIV_{WT}$ and $HIV_{A02}$ prompted us to further evaluate it against HIV-$2_{ROD}$ and $HIV_{DRV}{}^{R}{}_{P20}$. Antiviral assays using human MT-4 cells exposed to either HIV-$2_{ROD}$ or $HIV_{DRV}{}^{R}{}_{P20}$ showed that GRL008 was equipotent against $HIV_{WT}$ ($EC_{50}$, 0.038 μM) and HIV-$2_{ROD}$ ($EC_{50}$, 0.03 μM). LPV showed slightly better antiviral activity ($EC_{50}$, 0.014 μM) than GRL008 against HIV-$2_{ROD}$. Both TPV and RTV showed lesser antiviral activities against HIV-$2_{ROD}$, with $EC_{50}$s of 1.8 μM and 0.26 μM, respectively. While DRV showed a 50-fold increase in its $EC_{50}$ against $HIV_{DRV}{}^{R}{}_{P20}$ (0.05 μM) compared to its $EC_{50}$ against $HIV_{WT}$ (0.001 μM), GRL008 showed only a 2.6-fold increase in its $EC_{50}$ against $HIV_{DRV}{}^{R}{}_{P20}$ (0.097 μM) compared to its $EC_{50}$ against $HIV_{WT}$ (0.038 μM). TPV showed a 2.7-fold increase in its $EC_{50}$ against $HIV_{DRV}{}^{R}{}_{P20}$ (0.34 μM) compared to its $EC_{50}$ against $HIV_{WT}$ (0.128 μM). However, GRL008 showed a 3.5-fold-greater antiviral activity

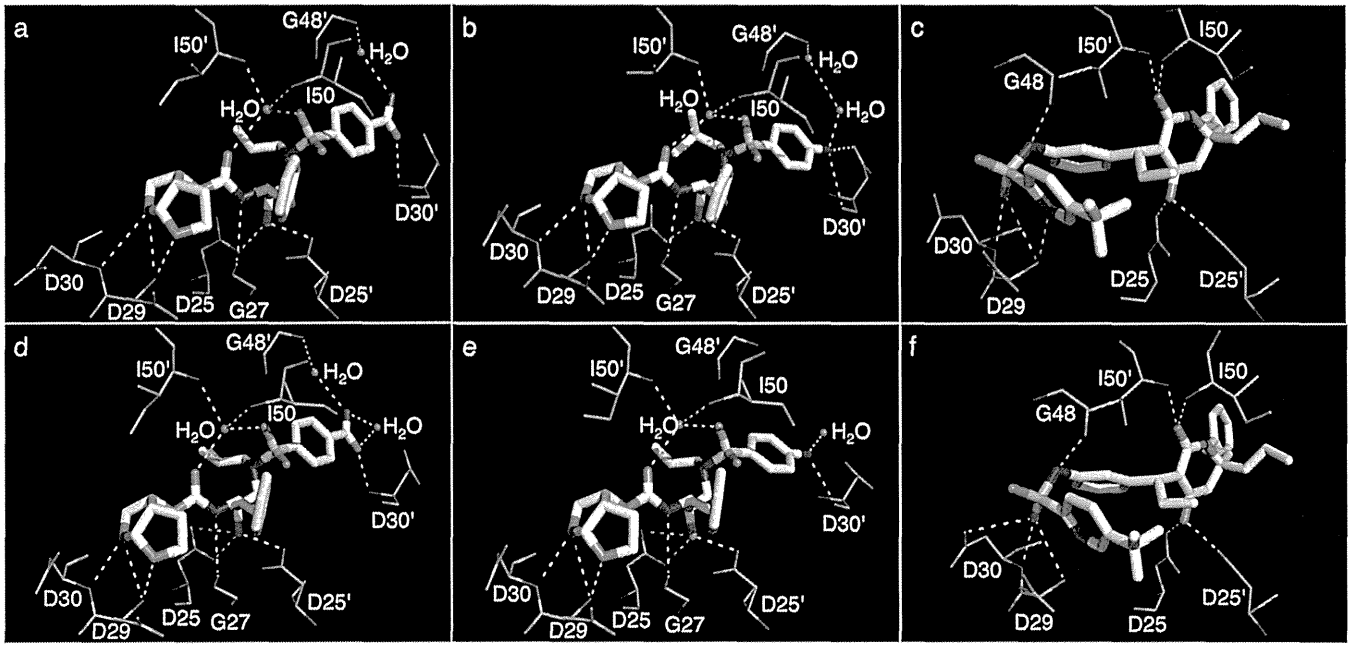


FIG 2 Hydrogen bonding profiles of GRL008, DRV, and TPV. H-bonds formed by GRL008, DRV, and TPV with $PR_{WT}$ (a, b, and c, respectively) and with $PR_{A02}$ (d, e, and f, respectively) in their corresponding crystal structures are shown as yellow dashed lines. In all panels, the carbon atoms of the inhibitors are shown as white thick sticks, while the corresponding carbon atoms of $PR_{WT}$ and $PR_{A02}$ residues are shown as green and cyan thin sticks, respectively. Nitrogen, oxygen, sulfur, and fluorine atoms are shown as blue, red, yellow, and light cyan sticks, respectively. Crystallographic water molecules are shown as red spheres. All H-bonds were calculated as the distances between two heavy atoms, with a maximum distance cutoff of 3.0 Å and minimum angle cutoff for donor of 90° and for acceptor of 60°. The P2 *bis*-THF moiety of GRL008 and DRV shows three conserved H-bonds with the backbone amide nitrogen atoms of D29 and D30 in both $PR_{WT}$ (a and b) and $PR_{A02}$ (d and e). While TPV shows similar three H-bonds with the backbone amide nitrogen atoms of D29 and D30 in $PR_{WT}$ (c), the sulfonyl oxygen of TPV shows two H-bonds, one each with the backbone amide nitrogen atoms of D29 and D30 and one H-bond with the side chain δ-oxygen atom of D30 from $PR_{A02}$ (f). Additionally, the P2′ moieties of GRL008 and DRV show one conserved H-bond, each with the backbone of D30′ (a, b, d, and e). Both GRL008 and DRV have a direct H-bond with the backbone carbonyl oxygen atom of G27 (a, b, d, and e). No H-bonds with D30′ or G27 were seen with TPV; instead, three direct H-bonds, one each with the backbone carbonyl oxygen atom of G48 and the backbone amide nitrogen atoms of I50 and I50′, were seen with TPV (c and f). In the cases of GRL008 and DRV, bridging H-bonds were seen with the backbone amide nitrogen atoms of I50 and I50′ via a conserved water molecule (a, b, d, and e). While the P2′ benzene carboxamide moiety of GRL008 showed a conserved bridging H-bond with G48′ from both $PR_{WT}$ and $PR_{A02}$ via a water molecule (a and d, respectively), such conserved bridging H-bonds were not seen for the P2′ aniline moiety of DRV with G48′ of $PR_{A02}$ (e). Overall, no significant changes in the H-bonding profiles were seen for GRL008, DRV, and TPV against $PR_{A02}$ compared to their profiles against $PR_{WT}$ in their respective crystal structures.

against $HIV_{DRV}{}^{R}{}_{P20}$ than TPV. RTV failed to inhibit $HIV_{DRV}{}^{R}{}_{P20}$ even at a 1.0 μM concentration. These results suggest that GRL008 has a greater genetic barrier than most of the PIs evaluated in this study.

**Crystal structures of $PR_{A02}$ in complex with PIs.** Crystal structures of $PR_{A02}$ in complex with GRL008, RTV, or TPV were solved to a resolution of 1.8 Å, while the structure of $PR_{A02}$ in complex with DRV was solved to a resolution of 1.95 Å (Table 2). All structures were solved in the space group $P2_1$, with two dimers of $PR_{A02}$ per asymmetric unit (AU), in agreement with the predicted number of $PR_{A02}$ dimers per Matthew's coefficient values (25), which were precalculated before molecular replacement. As shown in Fig. S1a, in the supplemental material, the overall *R* factors (wRfac), as calculated using MOLREP, were high, with low scores when one $PR_{A02}$ dimer per AU was obtained as a solution. When two dimers of $PR_{A02}$ per AU were obtained as a solution, the wRfac values decreased, with a relatively proportional increase in the corresponding scores (see Fig. S1a) for each of the structure solutions. No significant root mean square deviation (RMSD) in the $C_\alpha$ atoms of the two $PR_{A02}$ dimers within the AU was observed for any of the four structure solutions (see Fig. S1b). RMSD values of <1.0 Å were considered biologically insignificant. Continuous difference electron density was observed for GRL008, DRV, RTV, and TPV, with map correlation coefficient values of 0.94, 0.89, 0.78, and 0.88, respectively, in their corresponding maps. Based on the electron density maps, one molecule of GRL008, DRV, or TPV was fit into the active site of each $PR_{A02}$ dimer. On the other hand, two molecules of RTV were fit into the active site of each $PR_{A02}$ dimer. Thus, two molecules of GRL008, DRV, or TPV were fit per AU, while four molecules of RTV were fit per AU. The $R_{cryst}$ and $R_{free}$ values improved significantly (see Fig. S1c and d, respectively) with the two-step refinement of structure solutions containing two $PR_{A02}$ dimers per AU. The RMSDs in bond lengths and bond angles significantly improved (Table 2) by using the libraries for ligands that were geometry optimized through the semiempirical quantum mechanical method of refinement, eLBOW-AM1 (26) during refinement conducted using phenix.refine. Ramachandran plots showed no significant deviations for the protein, suggesting an overall good quality of stereochemistry.

**GRL008, DRV, and TPV showed minor changes in their binding profiles in the active site of $PR_{A02}$ compared to their interactions with $PR_{WT}$.** Crystal structures of $PR_{A02}$ in complex with GRL008, DRV, or TPV showed two $PR_{A02}$ dimers per AU, with each $PR_{A02}$ dimer bound to one molecule of the PI. No major

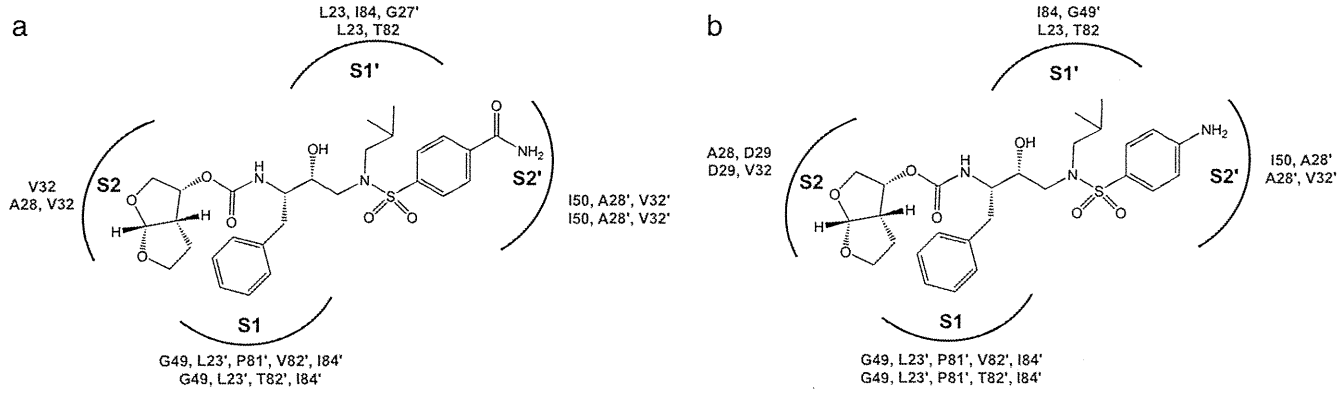


**FIG 3** Hydrophobic interactions of GRL008 and DRV. (a and b) Profiles of hydrophobic interactions for GRL008 (a) and DRV (b) in the active site of $PR_{A02}$ and $PR_{WT}$. The protease binding pockets (S2, S1, S1′, and S2′) are shown as arcs and are labeled. The corresponding protease amino acids that form the hydrophobic contacts with either GRL008 or DRV are listed for each binding pocket accordingly. Residues shown in green are from $PR_{WT}$ structures (PDB IDs 4I8Z and 4HLA for GRL008 and DRV, respectively), while the residues in red are from $PR_{A02}$. In both panels, the amino acid residues are labeled 1 to 99 for monomer 1 and 1′ to 99′ for monomer 2. Both GRL008 and DRV showed slightly altered but persistent contacts in all the binding pockets that were comparable to their corresponding wild-type profiles, thus supporting their higher antiviral activities.

differences in the binding profiles of three PIs were seen between the two $PR_{A02}$ dimers (within the AU) in their corresponding structures. As shown in Fig. 2, the P2 *bis*-THF moiety of GRL008 (panel d) and DRV (panel e) showed three strong H-bonds with the backbone amide nitrogen atoms of D29 (two contacts) and D30 (one contact). In the case of TPV, two strong H-bonds, one each with the backbone amide nitrogen atoms of D29 and D30, were seen (Fig. 2f). TPV showed two additional H-bonds in the S2 binding pocket of $PR_{A02}$, one with the backbone carbonyl oxygen atom of G48 and one with the side chain δ-oxygen atom of D30 (Fig. 2f). One strong H-bond with G27 was seen for both GRL008 and DRV but not for TPV. The P2′ moieties, benzene carboxamide (GRL008) and aniline (DRV), showed one strong H-bond each with the backbone amide nitrogen and the backbone carbonyl oxygen atoms of D30′, respectively. TPV, due to lack of P2′ polar atoms, did not show any H-bonds in the S2′ binding pocket of $PR_{A02}$. The transition-state mimic hydroxyl group of all three PIs showed at least one H-bond each with the δ-oxygen atoms from the side chains of both D25 and D25′ (Fig. 2d, e, and f). Both GRL008 and DRV showed two H-bonds each, with a conserved bridging water molecule, which in turn had H-bonds with the backbone amide nitrogen atoms of the $PR_{A02}$ flap residues, I50 and I50′ (Fig. 2d and e). TPV showed direct H-bonds with I50 and I50′ (Fig. 2f) without a bridging water molecule, as seen in its corresponding wild-type protease structure (PDB ID 2O4P) (Fig. 2c). In addition, the P2′ moieties of GRL008 and DRV showed H-bonds with two and one water molecules, respectively. In the case of GRL008, one of the water molecules, interacting with its P2′ moiety, showed a bridging H-bond with the backbone amide nitrogen atom of G48′ (Fig. 2d). As shown in Fig. 2a, a similar profile was seen in the crystal structure of $PR_{WT}$ in complex with GRL008 (PDB ID 4I8Z). As shown in Fig. 2b, DRV showed two water molecules and an H-bonding network between the P2′ aniline moiety and G48′ of $PR_{WT}$ (PDB ID 4HLA). However, as shown in Fig. 2e, such an H-bonding network was not seen in the crystal structure of $PR_{A02}$ in complex with DRV (PDB ID 4NJT). No major changes in the binding orientation were seen for any of the three PIs compared to their corresponding binding profiles against $PR_{WT}$.

As shown in Fig. 3, both GRL008 and DRV showed conserved hydrophobic interactions with residues L23, V32, G49, T82, L23′, A28′, V32′, T82′, and I84′ in the corresponding S1, S2, S1′, and S2′ binding pockets of $PR_{A02}$. GRL008 showed additional hydrophobic interactions with residues A28 and I50, while DRV showed additional hydrophobic interactions with residues D29 and P81′. Overall, the profiles of hydrophobic contacts for GRL008 and DRV were similar to their corresponding profiles against $PR_{WT}$ structures, PDB IDs 4I8Z and 4HLA, respectively. TPV is involved in multiple hydrophobic interactions with residues R8, L23, A28, D29, V32, G49, I50, P81, T82, R8′, G27′, A28′, V32′, G49′, I50′, and I84′ in the corresponding S1, S2, S1′, and S2′ binding pockets of $PR_{A02}$. No significant deviation was seen in the profile of hydrophobic contacts for TPV against $PR_{A02}$ compared to its corresponding profile against $PR_{WT}$ structure (PDB ID 2O4P). Thus, the binding profiles of GRL008, DRV, and TPV in the active site of $PR_{A02}$ were comparable to their corresponding profiles in the active site of $PR_{WT}$.

**RTV shows an altered binding orientation in the active site of $PR_{A02}$.** The crystal structure of $PR_{A02}$ in complex with RTV showed two $PR_{A02}$ dimers per AU. As shown in Fig. 4a and b, the P2′ thiazolyl moiety of RTV showed two alternate binding orientations, RTV-1 and RTV-2, in the active site of $PR_{A02}$. Superposition of RTV-1 onto RTV-2 is shown in Fig. S2 in the supplemental material for clarity. RTV-1 (Fig. 4a) showed a previously reported binding orientation seen in the active site of $PR_{WT}$ (PDB ID 1HXW). RTV-2 (Fig. 4b) shows the altered binding of the P2′ thiazolyl moiety, which contributes to a significant loss of contacts in the S2 and S2′ binding pockets of $PR_{A02}$. In order to verify the alternate conformations of the P2′ thiazolyl group of RTV, the average individual *B* factors of all five atoms (C1, C2, S3, C4, and N5) from the P2′ thiazolyl group were analyzed (see Fig. S3 in the supplemental material) and it was found that the individual *B* factors support the two conformations.

Two conserved H-bonds, one with the backbone amide nitrogen atom of D29 and one with the backbone carbonyl oxygen atom of G48, were seen for both RTV-1 and RTV-2 in the S2 binding pocket of $PR_{A02}$. Two and one H-bonds were seen with the backbone carbonyl oxygen atoms of G27 and G27′, respectively, for both RTV-1 and RTV-2. The

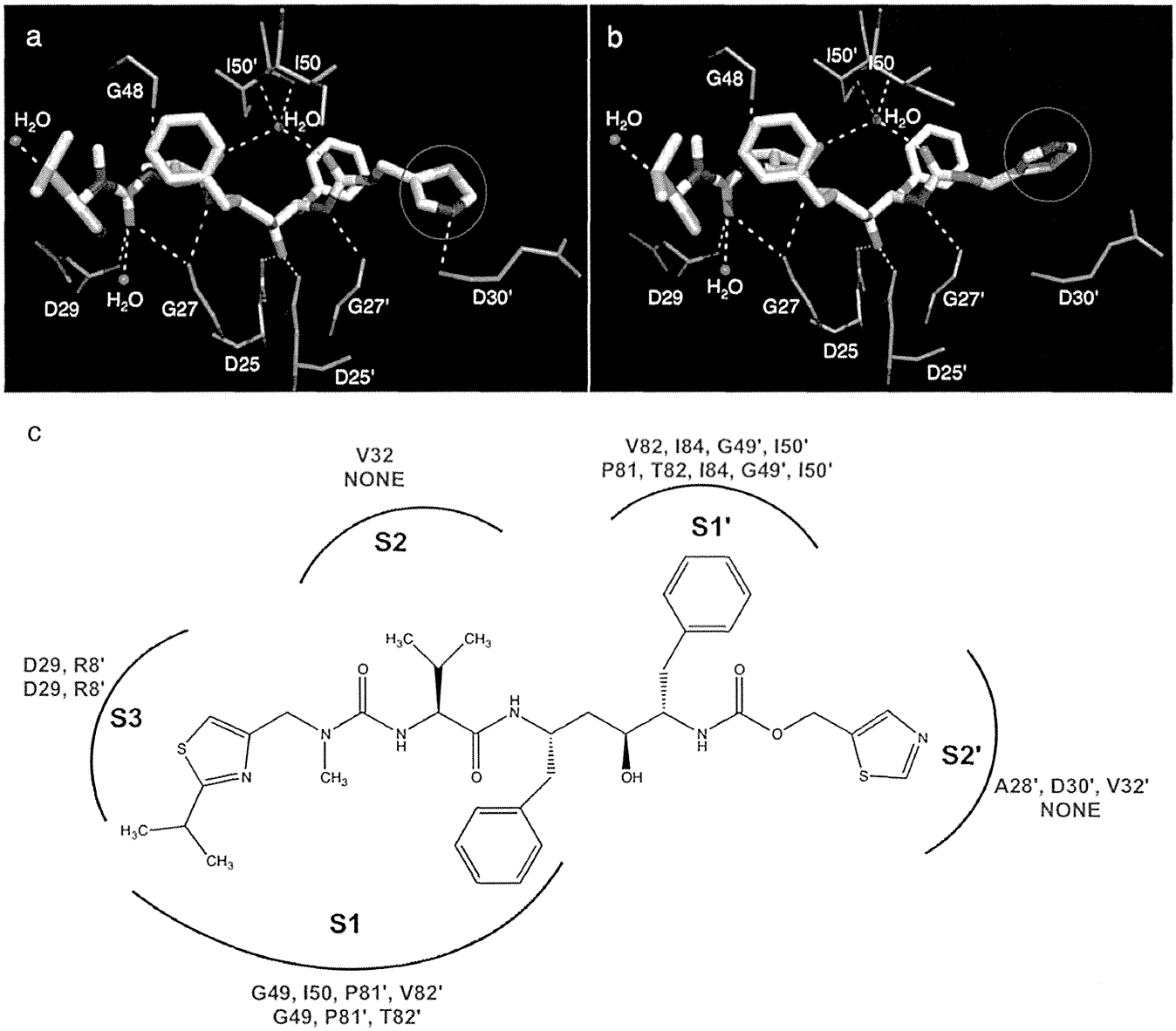


FIG 4 Hydrogen bonds and hydrophobic contacts for RTV in the active site of $PR_{A02}$. (a and b) H-bonds made by RTV-1 (a) and RTV-2 (b) (alternate conformations of the P2′ thiazolyl moiety of RTV, highlighted by red circles) in the active site of $PR_{A02}$. In both panels, the carbon atoms of RTV are shown as white thick sticks, while the carbon atoms of corresponding amino acid residues from $PR_{A02}$ are shown as green thin sticks. Nitrogen, oxygen, and sulfur atoms are shown as blue, red, and yellow sticks, respectively. Crystallographic water molecules are shown as red spheres, and the H-bonds are shown as yellow dashed lines. While RTV-1 (a) showed a profile comparable to its corresponding profile with $PR_{WT}$ (PDB ID 1HXW), RTV-2 (b) showed an altered binding orientation for the P2′ thiazolyl group, with an average root mean square deviation of 3 Å, resulting in loss of a critical H-bond with the backbone carbonyl oxygen atom of D30′. The P3 isopropyl group also showed a slightly altered binding orientation but was not biologically significant. (c) Profile of hydrophobic contacts made by RTV in the active sites of $PR_{WT}$ and $PR_{A02}$. The binding pockets are represented as arcs and are labeled accordingly. The corresponding amino acids from $PR_{WT}$ and $PR_{A02}$ that are involved in hydrophobic interactions with RTV are shown in green and red, respectively. For $PR_{A02}$, only RTV-2 is shown here because the binding profile of RTV-1 in the active site of $PR_{A02}$ is similar to that of its corresponding profile in the active site of $PR_{WT}$. RTV-2 showed significant loss of contacts in the S2 and S2′ binding pockets of $PR_{A02}$, thus supporting its weaker antiviral activity. Superposition of RTV-1 and RTV-2 is shown in Fig. S2 of the *supplemental material*.

transition-state mimic hydroxyl group of both RTV-1 and RTV-2 showed one H-bond each with the side-chain δ-oxygen atoms of both D25 and D25′. The P2′ thiazolyl group of RTV-2 showed a significant change in the binding orientation, with an average RMSD of 3 Å compared to that of RTV-1, resulting in loss of a critical H-bond with the backbone carbonyl oxygen atom of D30′. Both RTV-1 and RTV-2 showed a conserved water molecule that bridges H-bonds between RTV and the backbone amide nitrogen atoms of I50 and I50′. Two additional water molecules were seen for both RTV-1 and RTV-2 that are involved in H-bonding with the P3 and P2 moieties of RTV. Overall, the profiles of H-bonds for both RTV-1 and RTV-2 were similar to that of the wild-type structure (PDB ID 1HXW). However, the P2′ moiety of RTV-2 showed major conformational changes that resulted in the loss of a critical H-bond with D30′.

As shown in Fig. 4c, RTV-1 showed a profile of hydrophobic contacts similar to that of RTV, based on the $PR_{WT}$ crystal structure (PDB ID 1HXW), while RTV-2 showed loss of hydrophobic contacts in the S1, S2, and S2′ binding pockets of $PR_{A02}$. The isopropyl group from the P3 isopropylthiazolyl moiety showed minor changes in binding orientation, with an average RMSD of 1 Å, but still maintained hydrophobic contacts with Pro81. Nine amino acids (D29, G49, T82, I84, R8′, G49′ I50′, P81′, and T82′) from the S3, S1, and S1′ binding pockets of $PR_{A02}$ showed conserved hydrophobic interactions with both RTV-1 and RTV-2. RTV-2 showed complete loss of hydrophobic contacts in the S2 and S2′ binding pockets of $PR_{A02}$. Thus, the loss of contacts in the S1, S2, and S2′ binding pockets of $PR_{A02}$ should well explain the loss of antiviral activity of RTV against $HIV_{A02}$.

## DISCUSSION

The present structure-function data provide insights into the structural basis for the greater antiviral activity of a P2 *bis*-THF-containing novel PI, GRL008, and should help us understand the drug resistance mechanism of the clinical isolate $HIV_{A02}$ toward RTV and other PIs. $HIV_{A02}$ was initially isolated at the National Institutes of Health Clinical Center from a treatment-experienced male patient (age 44 years) who had been heavily treated with the PIs IDV, RTV, and SQV, along with reverse transcriptase (RT) inhibitors abacavir (ABC), 3′-azido-2′-dideoxythymidine (AZT), 2′,3′-dideoxyinosine (ddI), 3′-thiacytidine (3TC), 2′,3′-dideoxycytidine (ddC), and 2′,3′-didehydro-2′,3′-dideoxythymidine (d4T), as a part of 39-month antiviral therapy (10). Antiviral assays with viral isolates obtained by culturing the peripheral blood mononuclear cells (PBMCs) from the patient's blood sample showed 4- to >5,000-fold-increased resistance against IDV, RTV, SQV, and the RT inhibitors mentioned above (10). In the present study, the antiviral assays showed that both GRL008 and DRV, which contain the *bis*-THF group as the P2 moiety, were highly active with a desirable genetic barrier against $HIV_{A02}$, with no significant change in their $EC_{50}$s against $HIV_{A02}$ compared to those against $HIV_{WT}$. LPV was much less effective in inhibiting the replication of $HIV_{A02}$ than inhibiting $HIV_{WT}$ replication in the cell-based antiviral assays. The lower antiviral activity of LPV against $HIV_{A02}$ could be partially attributed to its structural resemblance to RTV, which was used in the treatment regimen of the patient described above. Although TPV was able to inhibit the replication of $HIV_{A02}$, GRL008 was found to be >12-fold more potent than TPV in this cell-based antiviral assay. As predicted, $HIV_{A02}$ was resistant to IDV, RTV, and SQV, in view of the fact that the patient failed the treatment with these three PIs. Achievement of higher anti-HIV-1 activity and a greater genetic barrier in combination with lower cytotoxicity and high oral bioavailability represent major critical goals in the design of novel PIs. For example, TMC-126, an analog of DRV that contains P2 *bis*-THF and P2′ methoxy benzene groups, was previously shown to have a greater antiviral potency than DRV, with a desirable genetic barrier (27), but could not be used further due to its poor oral bioavailability. Similarly, GRL007 (an analog of GRL008) showed poor cell penetration properties in spite of its picomolar enzyme inhibitory activity (9). It is noteworthy that GRL008 has a desirable therapeutic window due to its greater antiviral activity, lower cytotoxicity (50% cytotoxic concentration, >100 μM), and greater cell penetration capability, similar to that of DRV (9), thus making it a desirable compound to be further evaluated against multi-PI-resistant strains of HIV-1, including DRV-resistant strains.

It was previously noted that DRV resistance-associated amino acid substitutions are not clinically seen and the correlation for the occurrence of such DRV resistance-associated amino acid substitutions in conjunction with other PI resistance amino acid substitutions (such as L10I, I54V, V82T, and L90M, which are seen in $PR_{A02}$) is very low (8). However, we recently selected a highly DRV-resistant strain of HIV-1 *in vitro* by using a mixture of multi-PI-resistant (but DRV-sensitive) clinical HIV-1 strains as a starting viral population (7). In an attempt to examine the genetic barrier of GRL008, it was further evaluated against one of the DRV-resistant HIV-1 variants, $HIV_{DRV^{R}P20}$ (7) and was found to be potent, with only a 2.6-fold increase in its $EC_{50}$ above that for $HIV_{WT}$. Although TPV showed a similar 2.7-fold increase in its $EC_{50}$ against $HIV_{DRV^{R}P20}$, the absolute $EC_{50}$ of GRL008 was 3.5-fold lower than that of TPV, suggesting that GRL008 is overall a better PI than TPV against $HIV_{DRV^{R}P20}$.

The P2 *bis*-THF moiety of both GRL008 and DRV showed strong H-bonds with the backbone of conserved active-site amino acids D29 and D30 of $PR_{A02}$. The P2′ benzene carboxamide moiety of GRL008 was designed to replace one of the bridging water molecules seen with DRV (Fig. 2a and b) in the S2′ pocket (9). In the present study, the crystal structure of $PR_{A02}$ in complex with GRL008 showed a conserved profile of a bridging H-bond with G48′ via a water molecule (Fig. 2d), as was seen in its corresponding interactions with $PR_{WT}$ (PDB ID 4I8Z) (Fig. 2a). This suggests that the amino acid substitutions in $PR_{A02}$ do not affect the binding profile of GRL008 in either the S2 or S2′ binding pockets of $PR_{A02}$. On the other hand, of the two bridging water molecules in the S2′ pocket of $PR_{WT}$ in complex with DRV (PDB ID 4HLA) (Fig. 2b), only one was seen in the structure of $PR_{A02}$ in complex with DRV (Fig. 2e). Taken together, the crystal structures confirmed that both GRL008 and DRV, bound in the active site of $PR_{A02}$, do not have notable changes in their binding orientations; this evidence thus supports their greater conserved antiviral activities. These structural analyses may further explain in part the conserved and greater antiviral activity of GRL008 against $HIV_{DRV^{R}P20}$.

The crystal structure of $PR_{A02}$ in complex with TPV did not show major changes in the binding orientation of TPV (Fig. 2f) compared to that with $PR_{WT}$ (PDB ID 2O4P) (Fig. 2c). However, the $EC_{50}$ of TPV against $HIV_{A02}$ was >12-fold greater than that of GRL008. The P2′ region of TPV lacks polar groups, and hence no H-bonds were seen in the S2′ binding pocket of either $PR_{A02}$ or $PR_{WT}$, while both GRL008 and DRV showed persistent, strong H-bonds with the backbone of D30′ in the S2′ binding pocket of $PR_{A02}$. TPV has been shown to have a greater genetic barrier against multi-PI-resistant HIV-1 variants due to its unique mechanism of minor loss of binding affinity through entropy/enthalpy compensation against amino acid substitutions in the protease (28). In the present study, TPV showed a 2.8-fold change in its $EC_{50}$ against $HIV_{A02}$ versus $HIV_{WT}$, while GRL008 and DRV showed <1- and 2-fold changes, respectively, in their $EC_{50}$s against $HIV_{A02}$. Furthermore, based on Lipinski's rule of five (29) and the logP values of TPV (7.0) and DRV (2.9) obtained from the PubChem database (http://pubchem.ncbi.nlm.nih.gov/), it is apparent that DRV and analogs such as GRL008 have favorable oral bioavailabilities in addition to greater antiviral potencies than TPV against $HIV_{A02}$.

In this study, IDV, RTV, and SQV showed much lower antiviral activities against $HIV_{A02}$ than against $HIV_{WT}$ (Table 1). In particular, RTV showed a >29-fold increase in its $EC_{50}$ against $HIV_{A02}$ compared to its $EC_{50}$ against $HIV_{WT}$. In order to understand the RTV resistance mechanism of $HIV_{A02}$, the crystal structure of $PR_{A02}$ in complex with RTV was solved and analyzed. Morissette et al. previously showed that RTV undergoes a conformational polymorphism (30) that lowers its solubility and compromises its anti-HIV-1 activity. In the present study, the $EC_{50}$ of RTV against $HIV_{WT}$ (Table 1) was within 2-fold of the $EC_{50}$s of LPV, IDV, and SQV against $HIV_{WT}$, suggesting that the lowered solubility of RTV may not play a critical role in the loss of its activity against $HIV_{A02}$. The crystal structure of $PR_{A02}$ in complex with RTV showed an altered binding orientation of the P2′ thiazolyl moiety of RTV in the S2′ binding pocket of $PR_{A02}$ (Fig. 4a and b), with an RMSD of 3 Å. In order to understand the binding profiles of RTV, the crystal structure of $PR_{A02}$ in complex with RTV was compared in detail to its corresponding wild-type structure (PDB ID 1HXW). In the case of the $PR_{A02}$ structure, the H-bond between the P2′ thiazolyl group of RTV and D30′ was seen for RTV-1 (Fig. 4a), which closely resembled its corresponding binding orientation in the active site of $PR_{WT}$ (PDB ID 1HXW). On the other hand, the H-bond between the P2′ thiazolyl moiety of RTV-2 and D30′ of $PR_{A02}$ was lost (Fig. 4b). This loss of contact was not seen in the case of RTV interactions with $PR_{WT}$ (PDB ID 1HXW), suggesting that the conformational polymorphism of RTV may not be the reason for loss of its antiviral activity against $HIV_{A02}$.

Based on the binding profile of RTV-1, one could hypothesize that RTV-1 (Fig. 4a) inhibits the replication of $HIV_{A02}$ at least by 50% due to its close resemblance to its corresponding wild-type structure (PDB ID IHXW). However, it has been shown previously that the presence of less than 25% of active viral protease can support viral propagation, due to the formation of mature and infectious viral particles (31). Additionally, mutations at codons 10, 54, 63, 71, 82, and 84 have been known to cause HIV-1 resistance against RTV (32), and $PR_{A02}$ consists of amino acid substitutions L10I, I54V, L63P, A71V, and V82T. The combination of active-site and non-active-site amino acid substitutions has been shown to cause a significant loss of binding affinity to RTV (42- to 1,330-fold increase in the $K_i$ values compared to that for $PR_{WT}$) due to loss of direct contacts as well as altered protease-flap dynamics (33, 34). As shown in Fig. 4b, RTV-2 has a complete loss of direct contacts in the S2 and S2′ binding pockets of $PR_{A02}$. Furthermore, the substitution L63P has been previously shown to enhance viral fitness in combination with L90M (35). $PR_{A02}$ contains both amino acid substitutions L63P and L90M. Thus, the enhanced replication fitness of $HIV_{A02}$ in combination with loss of contacts for RTV in the active site of $PR_{A02}$ may well explain the compromised activity of RTV ($EC_{50}$, >1 μM) against $HIV_{A02}$ in the antiviral assays. In the case of patients, a study based on the Abbott M97-720 trial showed that low-level viremia could persist at least for 7 years in patients on an LPV/RTV regimen, partially due to latent viral reservoirs (36). Based on our structural analysis, amino acid substitutions (both active site and non-active site) in $PR_{A02}$ caused an altered binding orientation of RTV in the active site, resulting in a significant loss of contacts in the S2 and S2′ binding pockets of $PR_{A02}$ and, consequently, causing HIV-1 resistance to RTV. Thus, our present data not only explain the mechanism for RTV resistance but also help explain the retained antiviral potency of a novel P2 *bis*-THF-containing PI (GRL008) against $HIV_{A02}$.

In conclusion, the conserved H-bonding network of P2 *bis*-THF-containing PIs, such as GRL008 and DRV, with the backbone of conserved active-site amino acids G27, D29, D30, and D30′ of $PR_{A02}$ and $PR_{WT}$ most likely contributes to their antiviral activities against $HIV_{A02}$ and $HIV_{WT}$, with minimal changes in the $EC_{50}$s. In particular, GRL008 proved to have a favorable antiviral activity against $HIV_{DRV^{R}P20}$, a finding that warrants further investigation.

## ACKNOWLEDGMENTS

This study was supported in part by the Intramural Research Program of the Center for Cancer Research, National Cancer Institute, National Institutes of Health (H.M.), by a grant for the Global Education and Research Center aiming at the control of AIDS (Global Center of Excellence supported by Monbu-Kagakusho), Promotion of AIDS Research from the Ministry of Health, Welfare, and Labor of Japan, by a grant to the Cooperative Research Project on Clinical and Epidemiological Studies of Emerging and Re-emerging Infectious Diseases (Renkei Jigyo; grant 78, Kumamoto University) of Monbukagakusho (H.M.), and by a grant from the National Institutes of Health (GM53386; A.K.G.).

We thank the Advanced Photon Source (APS) for X-ray diffraction data collection. Use of the APS was supported by the U.S. Department of Energy, Office of Science, Office of Basic Energy Sciences, under contract DE-AC02-06CH11357 (LS-CAT) and contract W-31-109-Eng-38 (SER-CAT). Use of LS-CAT sector 21 was supported by the Michigan Economic Development Corporation and the Michigan Technology Tri-Corridor (grant 085P1000817). Supporting institutions for SER-CAT may be found at www.ser-cat.org/members.html. We thank the NIH AIDS Research and Reference Reagent program for providing IDV, LPV, RTV, SQV, and TPV. This study utilized the high-performance computational capabilities of the Biowulf Linux cluster at the National Institutes of Health, Bethesda, MD (http://biowulf.nih.gov).

## REFERENCES

1. Kohl NE, Emini EA, Schleif WA, Davis LJ, Heimbach JC, Dixon RA, Scolnick EM, Sigal IS. 1988. Active human immunodeficiency virus protease is required for viral infectivity. Proc. Natl. Acad. Sci. U. S. A. 85:4686–4690. http://dx.doi.org/10.1073/pnas.85.13.4686.
2. Peng C, Ho BK, Chang TW, Chang NT. 1989. Role of human immunodeficiency virus type 1-specific protease in core protein maturation and viral infectivity. J. Virol. 63:2550–2556.
3. Shafer RW, Rhee SY, Pillay D, Miller V, Sandstrom P, Schapiro JM, Kuritzkes DR, Bennett D. 2007. HIV-1 protease and reverse transcriptase mutations for drug resistance surveillance. AIDS 21:215–223. http://dx.doi.org/10.1097/QAD.0b013e328011e691.
4. Yedidi RS, Proteasa G, Martinez JL, Vickrey JF, Martin PD, Wawrzak Z, Liu Z, Kovari IA, Kovari LC. 2011. Contribution of the 80s loop of HIV-1 protease to the multidrug-resistance mechanism: crystallographic study of MDR769 HIV-1 protease variants. Acta Crystallogr. D Biol. Crystallogr. 67:524–532. http://dx.doi.org/10.1107/S0907444911011541.
5. Koh Y, Nakata H, Maeda K, Ogata H, Bilcer G, Devasamudram T, Kincaid JF, Boross P, Wang Y-F, Tie Y, Volarath P, Gaddis L, Harrison RW, Weber IT, Ghosh AK, Mitsuya H. 2003. Novel bis-tetrahydrofuranylurethan-containing nonpeptidic protease inhibitor (PI) UIC-94017 (TMC114) with potent activity against multi-PI-resistant human immunodeficiency virus in vitro. Antimicrob. Agents Chemother. 47:3123–3129. http://dx.doi.org/10.1128/AAC.47.10.3123-3129.2003.
6. Ghosh AK, Anderson DD, Weber IT, Mitsuya H. 2012. Enhancing protein backbone binding: a fruitful concept for combating drug-resistant HIV. Angew. Chem. Int. Ed. Engl. 51:1778–1802. http://dx.doi.org/10.1002/anie.201102762.
7. Koh Y, Amano M, Towata T, Danish M, Leshchenko-Yashchuk S, Das D, Nakayama M, Tojo Y, Ghosh AK, Mitsuya H. 2010. In vitro selection of highly darunavir-resistant and replication-competent HIV-1 variants by using a mixture of clinical HIV-1 isolates resistant to multiple conven-

tional protease inhibitors. J. Virol. 84:11961–11969. http://dx.doi.org/10.1128/JVI.00967-10.
8. Mitsuya Y, Liu TF, Rhee SY, Fessel WJ, Shafer RW. 2007. Prevalence of darunavir resistance-associated mutations: patterns of occurrence and association with past treatment. J. Infect. Dis. 196:1177–1179. http://dx.doi.org/10.1086/521624.
9. Yedidi RS, Maeda K, Fyvie WS, Steffey M, Davis DA, Palmer I, Aoki M, Kaufman JD, Stahl SJ, Garimella H, Das D, Wingfield PT, Ghosh AK, Mitsuya H. 2013. P2′ benzene carboxylic acid moiety is associated with decrease in cellular uptake: evaluation of novel nonpeptidic HIV-1 protease inhibitors containing P2 bis-tetrahydrofuran moiety. Antimicrob. Agents Chemother. 57:4920–4927. http://dx.doi.org/10.1128/AAC.00868-13.
10. Yoshimura K, Kato R, Yusa K, Kavlick MF, Maroun V, Nguyen A, Mimoto T, Ueno T, Shintani M, Falloon J, Masur H, Hayashi H, Erickson J, Mitsuya H. 1999. JE-2147: a dipeptide protease inhibitor (PI) that potently inhibits multi-PI-resistant HIV-1. Proc. Natl. Acad. Sci. U. S. A. 96:8675–8680. http://dx.doi.org/10.1073/pnas.96.15.8675.
11. Davis DA, Brown CA, Singer KE, Wang V, Kaufman J, Stahl SJ, Wingfield P, Maeda K, Harada S, Yoshimura K, Kosalaraksa P, Mitsuya H, Yarchoan R. 2006. Inhibition of HIV-1 replication by a peptide dimerization inhibitor of HIV-1 protease. Antiviral Res. 72:89–99. http://dx.doi.org/10.1016/j.antiviral.2006.03.015.
12. Ghosh AK, Leshchenko S, Noetzel M. 2004. Stereoselective photochemical 1,3-dioxolane addition to 5-alkoxymethyl-2(5H)-furanone: synthesis of bis-tetrahydrofuranyl ligand for HIV protease inhibitor UIC-94017 (TMC-114). J. Org. Chem. 69:7822–7829. http://dx.doi.org/10.1021/jo049156y.
13. Otwinowski Z, Minor W. 1997. Processing of x-ray diffraction data collected in oscillation mode. Methods Enzymol. 276:307–326. http://dx.doi.org/10.1016/S0076-6879(97)76066-X.
14. Leslie AG. 2006. The integration of macromolecular diffraction data. Acta Crystallogr. D Biol. Crystallogr. 62:48–57. http://dx.doi.org/10.1107/S0907444905039107.
15. Evans P. 2006. Scaling and assessment of data quality. Acta Crystallogr. D Biol. Crystallogr. 62:72–82. http://dx.doi.org/10.1107/S0907444905036693.
16. Potterton E, Briggs P, Turkenburg M, Dodson E. 2003. A graphical user interface to the CCP4 program suite. Acta Crystallogr. D Biol. Crystallogr. 59:1131–1137. http://dx.doi.org/10.1107/S0907444903008126.
17. Winn MD, Ballard CC, Cowtan KD, Dodson EJ, Emsley P, Evans PR, Keegan RM, Krissinel EB, Leslie AGW, McCoy A, McNicholas SJ, Murshudov GN, Pannu NS, Potterton EA, Powell HR, Read RJ, Vagin A, Wilson KS. 2011. Overview of the CCP4 suite and current developments. Acta Crystallogr. D Biol. Crystallogr. 67:235–242. http://dx.doi.org/10.1107/S0907444910045749.
18. Vagin A, Teplyakov A. 1997. MOLREP: an automated program for molecular replacement. J. Appl. Crystallogr. 30:1022–1025. http://dx.doi.org/10.1107/S0021889897006766.
19. Long F, Vagin AA, Young P, Murshudov GN. 2008. BALBES: a molecular replacement pipeline. Acta Crystallogr. D Biol. Crystallogr. 64:125–132. http://dx.doi.org/10.1107/S0907444907050172.
20. Murshudov GN, Vagin AA, Dodson EJ. 1997. Refinement of macromolecular structures by the maximum-likelihood method. Acta Crystallogr. D Biol. Crystallogr. 53:240–255. http://dx.doi.org/10.1107/S0907444996012255.
21. Lamzin VS, Wilson KS. 1993. Automated refinement of protein models. Acta Crystallogr. D Biol. Crystallogr. 49:120–147. http://dx.doi.org/10.1107/S0907444992006747.
22. Zwart PH, Langer GG, Lamzin VS. 2004. Modelling bound ligands in protein crystal structures. Acta Crystallogr. D Biol. Crystallogr. 60:2230–2239. http://dx.doi.org/10.1107/S0907444904012995.
23. Schuttelkopf AW, van Aalten DMF. 2004. PRODRG: a tool for high throughput crystallography of protein-ligand complexes. Acta Crystallogr. D Biol. Crystallogr. 60:1355–1363. http://dx.doi.org/10.1107/S0907444904011679.
24. Adams PD, Afonine PV, Bunkoczi G, Chen VB, Davis IW, Echols N, Headd JJ, Hung L-W, Kapral GJ, Grosse-Kunstleve RW, McCoy AJ, Moriarty NW, Oeffner R, Read RJ, Richardson DC, Richardson JS, Terwilliger TC, Zwart PH. 2010. PHENIX: a comprehensive Python based system for macromolecular structure solution. Acta Crystallogr. D Biol. Crystallogr. 66:213–221. http://dx.doi.org/10.1107/S0907444909052925.
25. Matthews BW. 1968. Solvent content of protein crystals. J. Mol. Biol. 33:491–497. http://dx.doi.org/10.1016/0022-2836(68)90205-2.
26. Moriarty NW, Grosse-Kunstleve RW, Adams PD. 2009. Electronic Ligand Builder and Optimization Workbench (eLBOW): a tool for ligand coordinate and restraint generation. Acta Crystallogr. D Biol. Crystallogr. 65:1074–1080. http://dx.doi.org/10.1107/S0907444909029436.
27. Yoshimura K, Kato R, Kavlick MF, Nguyen A, Maroun V, Maeda K, Hussain KA, Ghosh AK, Gulnik SV, Erickson JW, Mitsuya H. 2002. A potent human immunodeficiency virus type 1 protease inhibitor, UIC-94003 (TMC-126), and selection of a novel (A28S) mutation in the protease active site. J. Virol. 76:1349–1358. http://dx.doi.org/10.1128/JVI.76.3.1349-1358.2002.
28. Muzammil S, Armstrong AA, Kang LW, Jakalian A, Bonneau PR, Schmelmer V, Amzel LM, Freire E. 2007. Unique thermodynamic response of tipranavir to human immunodeficiency virus type 1 protease drug resistance mutations. J. Virol. 81:5144–5154. http://dx.doi.org/10.1128/JVI.02706-06.
29. Lipinski CA, Lombardo F, Dominy BW, Feeney PJ. 2001. Experimental and computational approaches to estimate solubility and permeability in drug discovery and development settings. Adv. Drug Deliv. Rev. 46:3–26. http://dx.doi.org/10.1016/S0169-409X(00)00129-0.
30. Morissette SL, Soukasene S, Levinson D, Cima MJ, Almarsson O. 2003. Elucidation of crystal form diversity of the HIV protease inhibitor ritonavir by high-throughput cyrstallization. Proc. Natl. Acad. Sci. U. S. A. 100:2180–2184. http://dx.doi.org/10.1073/pnas.0437744100.
31. Rose JR, Babe LM, Craik CS. 1995. Defining the level of human immunodeficiency virus type 1 (HIV-1) protease activity required for HIV-1 particle maturation and infectivity. J. Virol. 69:2751–2758.
32. Schmit JC, Ruiz L, Clotet B, Raventos A, Tor J, Leonard J, Desmyter J, De Clercq E, Vandamme AM. 1996. Resistance-related mutations in the HIV-1 protease gene of patients treated for 1 year with the protease inhibitor ritonavir (ABT-538). AIDS 10:995–999. http://dx.doi.org/10.1097/00002030-199610090-00010.
33. Muzammil S, Ross P, Freire E. 2003. A major role for a set of non-active site mutations in the development of HIV-1 protease drug resistance. Biochemistry 42:631–638. http://dx.doi.org/10.1021/bi027019u.
34. Clemente JC, Moose RE, Hemrajani R, Whitford LRS, Govindasamy L, Reutzel R, McKenna R, Agbandje-McKenna M, Goodenow MM, Dunn BM. 2004. Comparing the accumulation of active- and nonactive-site mutations in the HIV-1 protease. Biochemistry 43:12141–12151. http://dx.doi.org/10.1021/bi049459m.
35. Martinez-Picado J, Savara AV, Sutton L, D'Aquila RT. 1999. Replication fitness of protease inhibitor-resistant mutants of human immunodeficiency virus type 1. J. Virol. 73:3744–3752.
36. Palmer S, Maldarelli F, Wiegand A, Bernstein B, Hanna GJ, Brun SC, Kempf DJ, Mellors JW, Coffin JM, King MS. 2008. Low-level viremia persists for at least 7 years in patients on suppressive antiretroviral therapy. Proc. Natl. Acad. Sci. U. S. A. 105:3879–3884. http://dx.doi.org/10.1073/pnas.0800050105.

# Dimerization of HIV-1 protease occurs through two steps relating to the mechanism of protease dimerization inhibition by darunavir

Hironori Hayashi[a,b], Nobutoki Takamune[c], Takashi Nirasawa[d], Manabu Aoki[a,e], Yoshihiko Morishita[d], Debananda Das[b], Yasuhiro Koh[a], Arun K. Ghosh[f], Shogo Misumi[c], and Hiroaki Mitsuya[a,b,1]

[a]Departments of Hematology, Rheumatology, and Infectious Disease, Kumamoto University Graduate School of Medicine, 1-1-1 Honjo, Chuo-ku, Kumamoto 860-8556, Japan; [b]Experimental Retrovirology Section, HIV and AIDS Malignancy Branch, National Cancer Institute, National Institutes of Health, Bethesda, MD 20892; [c]Department of Biochemistry, Kumamoto University Graduate School of Pharmaceutical Sciences, 5-1 Ooehonmachi, Chuo-ku, Kumamoto 862-0973, Japan; [d]Bruker Daltonics K.K., 3-9 Moriya, Kanagawa-ku, Yokohama 221-0022, Japan; [e]Department of Medical Technology, Kumamoto Health Science University, 325 Izumi-cho, Kita-ku, Kumamoto 861-5598, Japan; and [f]Departments of Chemistry and Medicinal Chemistry, Purdue University, West Lafayette, IN 47907

Edited* by Yoshihiro Kawaoka, University of Wisconsin–Madison, Madison, WI, and approved June 27, 2014 (received for review January 2, 2014)

**Dimerization of HIV-1 protease (PR) subunits is an essential process for PR's acquisition of proteolytic activity, which plays a critical role in the maturation of HIV-1. Recombinant wild-type PR ($PR^{WT}$) proved to dimerize, as examined with electrospray ionization mass spectrometry; however, two active site interface PR mutants ($PR^{T26A}$ and $PR^{R87K}$) remained monomeric. On the other hand, two termini interface PR mutants ($PR^{1\text{-}C95A}$ and $PR^{97/99}$) took both monomeric and dimeric forms. Differential scanning fluorimetry indicated that $PR^{1\text{-}C95A}$ and $PR^{97/99}$ dimers were substantially less stable than $PR^{WT}$ dimers. These data indicate that intermolecular interactions of two monomers occur first at the active site interface, generating unstable or transient dimers, and interactions at the termini interface subsequently occur, generating stable dimers. Darunavir (DRV), an HIV-1 protease inhibitor, inhibits not only proteolytic activity but also PR dimerization. DRV bound to protease monomers in a one-to-one molar ratio, inhibiting the first step of PR dimerization, whereas conventional protease inhibitors (such as saquinavir) that inhibit enzymatic activity but not dimerization failed to bind to monomers. DRV also bound to mutant PRs containing the transframe region-added PR (TFR-$PR^{D25N}$ and TFR-$PR^{D25N\text{-}7AA}$), whereas saquinavir did not bind to TFR-$PR^{D25N}$ or TFR-$PR^{D25N\text{-}7AA}$. Notably, DRV failed to bind to mutant PR containing four amino acid substitutions (V32I, L33F, I54M, and I84V) that confer resistance to DRV on HIV-1. To our knowledge, the present report represents the first demonstration of the two-step PR dimerization dynamics and the mechanism of dimerization inhibition by DRV, which should help design further, more potent novel PIs.**

AIDS | thermal stability | two-step dimerization dynamics | protease precursor

Dimerization of HIV-1 protease (PR) subunits is an essential process for the acquisition of proteolytic activity of PR, which plays a critical role in viral maturation in the replication cycle of HIV-1 (1, 2). Thus, PR dimerization inhibition is likely to abolish proteolytic activity and should serve as a promising target for HIV-1 intervention. Structurally there are two interfaces, which operate in the efficient PR dimerization. One is the termini interface, and the other is the active site interface (3, 4). The termini interface comprises four antiparallel β-sheets involving the first four amino- and carboxy-termini residues of both subunits. Todd et al. (5) have reported that the binding force generated by the termini interface contributes close to 75% of the entire dimerization energy. Indeed, Ishima and others have demonstrated that three amino acid substitutions (T26A, D29N, and R87K), located at the active site interface, together with C-terminal truncation of four amino acids (96–99), effectively disrupted PR dimerization as examined with NMR spectroscopy (Fig. 1) (6–8). Various groups have tried to target the termini interface in an attempt to intervene HIV-1 replication (9–12); however, none of such efforts to disrupt the termini interface interactions have led to clinical applications. On the other hand, the most recently US Food and Drug Administration (FDA)-approved PR inhibitor (PI), darunavir (DRV), is (to our knowledge) the first to be shown to block the dimerization of HIV-1 PR, as examined with the intermolecular FRET-based HIV-expression assay (Fig. S1) (13). Furthermore, a combination of four amino acid substitutions in the proximity of the active site interface (V32I/L33F/I54M/I84V), which emerged in PR when HIV-1–infected individuals were heavily treated with multiple PR inhibitors (PIs) and failed such treatment and when HIV-1 was selected in vitro in the presence of increasing concentrations of DRV (14), has been shown to decrease the dimerization inhibition activity of DRV (Fig. 1 and Fig. S1*B*) (15). However, the dynamics of dimerization of PR subunits, as well as the molecular mechanism of DRV inhibition of PR dimerization, remain to be elucidated.

Here we generated a variety of recombinant PR species with various amino acid substitution(s) and/or deletions introduced

## Significance

**Dimerization of HIV-1 protease (PR) plays a critical role in the replication of HIV-1. Darunavir (DRV) inhibits not only proteolytic activity but also PR dimerization. The present study shows that PR dimerization process undergoes two steps and that DRV inhibits the first step of PR dimerization by binding to PR monomers in a one-to-one molar ratio. The present study also demonstrates that DRV binds to a transframe precursor PR protein, indicating that DRV's monomer binding is involved in the Gag-Pol autoprocessing inhibition. To our knowledge, the present report represents the first demonstration of the two-step PR dimerization dynamics and the mechanism of dimerization inhibition by DRV, which should help design further, more potent novel PR inhibitors.**

Author contributions: H.H. and H.M. designed research; H.H., N.T., T.N., M.A., and Y.M. performed research; N.T., M.A., Y.M., and A.K.G. contributed new reagents/analytic tools; H.H., N.T., T.N., D.D., Y.K., S.M., and H.M. analyzed data; and H.H. and H.M. wrote the paper.

Conflict of interest statement: A.K.G. and H.M. are coinventors on a US government patent for darunavir. H.M. is an employee of the US government and is named so under the terms of the Federal Technology Transfer Act. All rights, title, and interest to the patent have been assigned to the US government, which may give a part of the royalties the government receives to its inventors.

*This Direct Submission article had a prearranged editor.

[1]To whom correspondence should be addressed. Email: hmitsuya@helix.nih.gov.

This article contains supporting information online at www.pnas.org/lookup/suppl/doi:10.1073/pnas.1400027111/-/DCSupplemental.

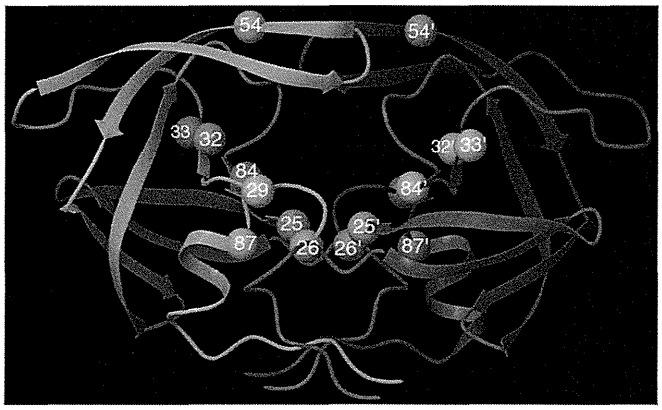


**Fig. 1.** Locations of major amino acid substitutions examined in the present study. V32I, L33F, I54M, and I84V are associated with HIV-1's DRV resistance. T26, D29, and R87 are known to be critical for PR dimerization. D25N is inserted to inactivate the enzymatic activity of HIV-1 PR.

and examined whether such mutated PR species interacted and dimerized using electrospray ionization mass spectrometry (ESI-MS) (16, 17). We also asked how PIs, including DRV, interacted with such various PR species and blocked the dimerization of PR subunits. The present data demonstrate that intermolecular interactions of two monomers occur first at the active site interface, generating weakly dimerized subunits (transient dimers), and that interactions at the termini interface subsequently occur, generating stable dimers. The ESI-MS data also show that DRV binds to PR monomers in a one-to-one molar ratio and inhibits the first step of PR dimerization, whereas conventional PIs (such as saquinavir) fail to bind to monomers. To our knowledge, the present report should represent the first demonstration of the two-step PR dimerization dynamics and the mechanism of dimerization inhibition by DRV.

## Results

The ESI-MS spectra of $PR^{WT}$ and $PR^{D25N}$ revealed four peaks of differently charged ions in the range of mass/charge ratio ($m/z$) of 1,500–2,500 (Fig. 2 *A* and *B*). Because +5 charged monomer ion and +10 charged dimer ion have the same $m/z$ ($m/z$ = 2,164.77 as calculated with their average mass in the case of $PR^{D25N}$), the greatest peak detected at $m/z$ 2,164.51 was determined to represent two forms, a PR monomer and PR dimer, thus being $[PR^{D25N}]^{5+}$ and $[2PR^{D25N}]^{10+}$ (Fig. S2*A*). In the present report hereafter, we designate a monomer and a dimer ion of $PR^{X}$ as $[PR^{X}]^{Y}$ and $[2PR^{X}]^{Y}$, respectively, where X denotes an amino acid substitution(s) and Y denotes a charge of ion. To determine whether the detected ions represented monomers and/or dimers, we examined multiply charged isotopologue clusters of $PR^{D25N}$ using the Solarix FT-ICR MS (Bruker Daltonics) and analyzed the difference in $m/z$ ratios of two adjacent isotope peaks ($\Delta m/z$) because monomer and dimer $PR^{D25N}$ ions with the same $m/z$ show different $\Delta m/z$ values in order of their charges (Figs. S2 and S3 and Table S1) (18). The results of isotopologue ion analysis, illustrated in Fig. S3 *A* and *B*, demonstrated that the ions observed at $m/z$ 1,546.39 and 1,803.94 in Fig. S2*A* were +7 and +6 charged monomer $PR^{D25N}$ ions ($[PR^{D25N}]^{7+}$ and $[PR^{D25N}]^{6+}$), respectively. The ions detected at $m/z$ 2,164.51 in Fig. S2*A* represent a mixture of +5 charged $PR^{D25N}$ monomers and +10 charged $PR^{D25N}$ dimers, designated as $[PR^{D25N}]^{5+}$ and $[2PR^{D25N}]^{10+}$, respectively, as shown in Fig. S3*D*, where "2PR" denotes a cluster of PR dimers. The ions at $m/z$ 1,967.84 and 2,404.91 in Fig. S2*A* represent +9 and +11 charged $PR^{D25N}$ dimers ($[2PR^{D25N}]^{11+}$ and $[2PR^{D25N}]^{9+}$), respectively, as shown in Fig. S3 *C* and *E*.

We also constructed three mutated PR species containing amino acid substitutions at the active site ($PR^{D29N}$, $PR^{T26A}$, and $PR^{R87K}$), a C terminus-truncated mutant ($PR^{1\text{-}C95A}$), and a PR carrying L97A and F99A substitutions ($PR^{97/99}$) (6, 19). In Fig. 2*C*, two $PR^{D29N}$ dimer ions ($[2PR^{D29N}]^{11+}$ and $[2PR^{D29N}]^{9+}$) were detected, whereas no dimer ions were detected with $PR^{T26A}$ and $PR^{R87K}$ (Fig. 2 *D* and *E*). Additional analyses of the isotopologue ion peaks with $PR^{T26A}$ and $PR^{R87K}$ confirmed the absence of dimer ions (Fig. S4 *A–F* and Table S1). Importantly, two $PR^{1\text{-}C95A}$ dimer ions ($[2PR^{1\text{-}C95A}]^{11+}$ and $[2PR^{1\text{-}C95A}]^{9+}$) were identified, although $PR^{1\text{-}C95A}$ monomer ion ($[PR^{1\text{-}C95A}]^{6+}$) was found to be a major peak (Fig. 2*F*). Two dimer ions were also detected in the case of $PR^{97/99}$, as shown in Fig. 3*C*. Considering that $[PR^{WT}]^{5+}$+$[2PR^{WT}]^{10+}$ representing monomers+dimers was found to be a major peak together with a minor peak of $[PR^{WT}]^{6+}$ in Fig. 2*A*, the $PR^{1\text{-}C95A}$ and $PR^{97/99}$ species were thought to have a significantly reduced but persistent ability to dimerize in comparison with $PR^{WT}$. Taken together, the data strongly suggest that the PR dimerization process consists of two distinct steps: (*i*) initial albeit weak intermolecular interactions occurring in the active site interface, constructing unstable or transient dimers, and (*ii*) subsequent interactions in the termini interface, resulting in the complete and tighter PR dimerization (Fig. 4).

In an attempt to examine the thermal stability of $PR^{WT}$ and various mutated PR species mentioned above, we conducted

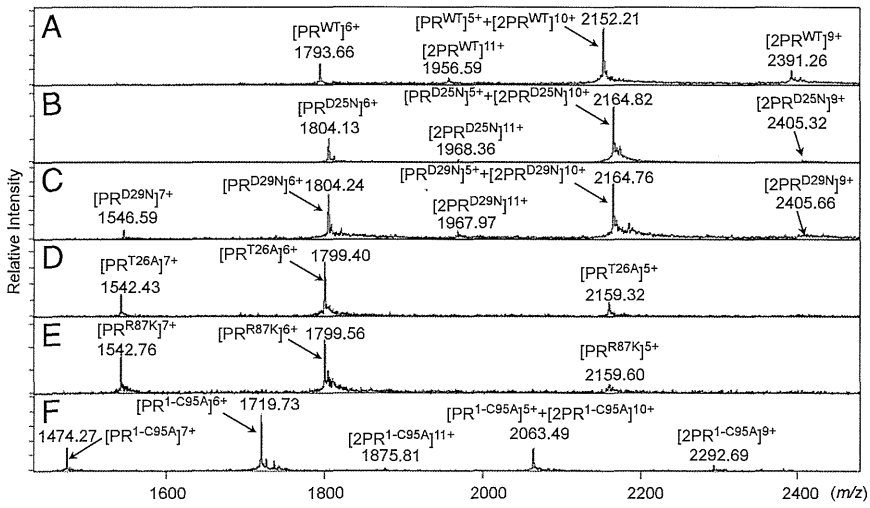


**Fig. 2.** ESI-MS spectra with $PR^{D25N}$, $PR^{D29N}$, $PR^{T26A}$, $PR^{R87K}$, and $PR^{1\text{-}C95A}$. (*A*) The ESI-MS spectrum of $PR^{WT}$ (10 μM). (*B–F*) Results of ESI-MS analysis of each mutant (10 μM). (*B*) The ESI-MS spectrum of $PR^{D25N}$ showed four peaks derived from its monomer and/or dimer ions. (*C*) $PR^{D29N}$ showed five peaks including +11 or +9 charged dimer ions. (*D* and *E*) The ESI-MS spectra of $PR^{T26A}$ and $PR^{R87K}$, respectively. The isotopologue ion peak analysis showed that all peaks detected in the ESI-MS spectra of $PR^{T26A}$ and $PR^{R87K}$ were derived from monomer ions (Fig. S4 and Table S1). (*F*) In the spectrum of $PR^{1\text{-}C95A}$, five peaks including the +11 and +9 charged dimer ions were seen. The average mass of $PR^{WT}$, $PR^{D25N}$, $PR^{D29N}$, $PR^{T26A}$, $PR^{R87K}$, and $PR^{1\text{-}C95A}$ are 10,755.76, 10,818.86, 10,818.86, 10,789.82, 10,791.83, and 10,312.24, respectively.